Published in final edited form as:

Cell Rep. 2020 May 12; 31(6): 107631. doi:10.1016/j.celrep.2020.107631.

In Vivo Cell Fate Tracing Provides No Evidence for Mesenchymal to Epithelial Transition in Adult Fallopian Tube and Uterus

Arnab Ghosh[1,2], **Shafiq M. Syed**[1,2], **Manish Kumar**[1,2], **Tyler J. Carpenter**[3], **Jose M. Teixeira**[3], **Nathaniel Houairia**[1,2], **Sumedha Negi**[1,2], **Pradeep S. Tanwar**[1,2,4,*]

[1]School of Biomedical Sciences and Pharmacy, University of Newcastle, Callaghan, NSW 2308, Australia

[2]Hunter Medical Research Institute, New Lambton Heights, NSW 2305, Australia

[3]Department of Obstetrics, Gynecology and Reproductive Biology, College of Human Medicine, Michigan State University, Grand Rapids, MI 49503, USA

[4]Lead Contact

SUMMARY

The mesenchymal to epithelial transition (MET) is thought to be involved in the maintenance, repair, and carcinogenesis of the fallopian tube (oviduct) and uterine epithelium. However, conclusive evidence for the conversion of mesenchymal cells to epithelial cells in these organs is lacking. Using embryonal cell lineage tracing with reporters driven by mesenchymal cell marker genes of the female reproductive tract (AMHR2, CSPG4, and PDGFRβ), we show that these reporters are also expressed by some oviductal and uterine epithelial cells at birth. These mesenchymal reporter-positive epithelial cells are maintained in adult mice across multiple pregnancies, respond to ovarian hormones, and form organoids. However, no labeled epithelial cells are present in any oviductal or uterine epithelia when mesenchymal cell labeling was induced in adult mice. Organoids developed from mice labeled in adulthood were also negative for mesenchymal reporters. Collectively, our work found no definitive evidence of MET in the adult fallopian tube and uterine epithelium.

Graphical Abstract

*Correspondence: pradeep.tanwar@newcastle.edu.au.

AUTHOR CONTRIBUTIONS

Conceptualization, A.G. and P.S.T.; Methodology, A.G., S.M.S., M.K., and P.S.T.; Investigation, A.G., S.M.S., and P.S.T.; Data Collection & Analysis, A.G., S.M.S., M.K., T.J.C., J.M.T, N.K., S.N., and P.S.T.; Writing – Review & Editing, A.G., S.M.S., J.M.T., and P.S.T.; Funding Acquisition, P.S.T.

DECLARATION OF INTERESTS

The authors declare no competing interests.

SUPPLEMENTAL INFORMATION

Supplemental Information can be found online at https://doi.org/10.1016/j.celrep.2020.107631.

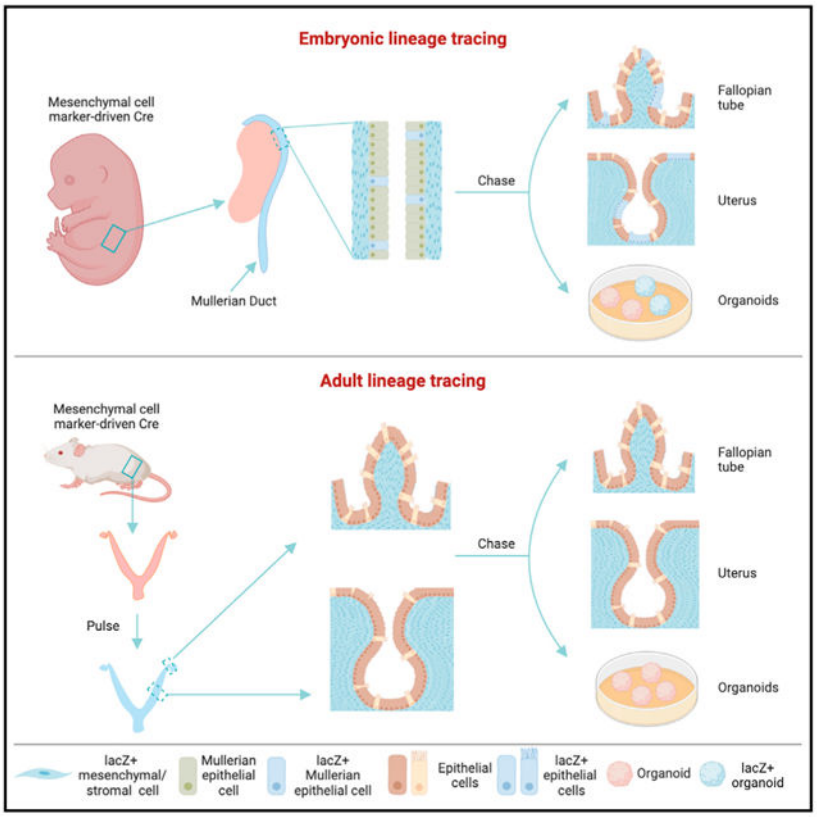

In Brief

Mesenchymal to epithelial transition (MET) is postulated to be involved in the maintenance and regeneration of the epithelium of female reproductive organs. Here, Ghosh et al. report no definitive evidence of MET in the adult epithelium of oviduct and uterus using *in vivo* cell lineage tracing and organoids.

INTRODUCTION

The mammalian female reproductive tract (FRT) is essential for fertility, and dysregulation in its functions contributes to many gynecological diseases, including ovarian cancer (Teixeira et al., 2001). The FRT develops from a pair of simple tubular structures known as müllerian ducts (MDs). The MDs are formed from the coelomic epithelium and, irrespective of genotypic sex, are present in both males and females (Mullen and Behringer, 2014; Teixeira et al., 2001). However, anti-Müllerian hormone (also known as Müllerian-inhibiting substance), secreted by the Sertoli cells of the fetal testes, causes regression of the MDs in males (Teixeira et al., 2001). In both humans and mice, the MD epithelium is mesoepithelial in nature because it expresses the mesenchymal markers, such as vimentin, in the epithelial cells. (Fritsch et al., 2013; Orvis and Behringer, 2007; Paranko and Virtanen, 1986). In females, the MDs undergo progressive differentiation with age in a caudal-to-cranial direction to acquire unique morphologic, organ-specific epithelial features and give rise to the fallopian tubes (FT) (oviducts in non-primates), uterus, cervix, and anterior portion of

the vagina (Fritsch et al., 2013; Teixeira et al., 2001). Postnatally, the epithelium of the MD-derived organs is more differentiated and expresses typical epithelial markers, such as cytokeratins (Fritsch et al., 2013; Peri et al., 2015; Song et al., 1998).

Mesenchymal to epithelial transition (MET) plays an essential role during embryonic development. Although there is limited evidence of MET in adult organs (Pei et al., 2019), there have been reports that suggest MET could be occurring in the FRT. For example, in the adult mouse uterus, stromal cells expressing the AMH type 2 receptor (AMHR2) or smooth muscle 22 α (SM22α, also called transgelin) have been shown to convert to epithelial cells during the repair and regeneration of the injured endometrium, and alterations in these cells contribute to endometrial hyperplasia (Huang et al., 2012; Owusu-Akyaw et al., 2019; Patterson et al., 2013; Yin et al., 2019). Interestingly, these AMHR2$^+$ or SM22α$^+$ stromal-cell-derived epithelial cells are generally not present in the normal endometrial epithelium and only appear after physical or postpartum injury (Huang et al., 2012; Patterson et al., 2013; Yin et al., 2019). Similarly, oviductal AMHR2$^+$ stromal cells have been shown to undergo epithelialization and, upon oncogenic transformation, develop serous ovarian cancer (Hua et al., 2016; Kim et al., 2012). These studies appear to challenge the more traditional view of the adult epithelial regeneration and carcinogenesis in which epithelial cells are known to have a central role (Daikoku et al., 2008, 2011; Ghosh et al., 2017; Perets et al., 2013; Russo et al., 2018; Sherman-Baustet al., 2014; Wu et al., 2016). As many of these MET studies used mesenchymal-cell-specific Cre reporters that are activated in the MDs during early embryonic development when MD epithelial cells have mesoepithelial characteristics and express mesenchymal markers, it is unclear whether the subsequent appearance of the reporter-labeled epithelial cells is due to the embryonic expression of Cre in the MD epithelium or because of MET. Additionally, some of the Cre reporters are also expressed in the coelomic epithelium, the precursor of MDs (Guioli et al., 2007; Orvis and Behringer, 2007).

Here, we performed lineage tracing of both epithelial and mesenchymal cells by inducing permanent reporter expression in these cells during embryonic and adult stages. This technique is a gold standard approach to track the behavior of labeled cells and their subsequent progenies in their native environment in tissues and organs (Chari et al., 2017; Kretzschmar and Watt, 2012). To investigate comprehensively the extent of MET in the FRT organs, we analyzed 10 different mouse models. First, we analyzed *Amhr2^{Cre};R26-lacZ$^{fl/+}$*, *Amhr2-lacZ*, and *Sm22^{Cre};R26-lacZ$^{fl/+}$* mice to replicate the results of previous studies. We screened for the presence of any *lacZ$^+$* cells in the oviduct and uterus after cutting the whole organs into 125-μm-thick, serial sections and also performed histopathological analysis using thin (5 μm) sections. Our analyses showed that *lacZ$^+$* cells are indeed present in the oviductal and uterine epithelium of neonatal, prepubertal, and adult *Amhr2^{Cre};R26-lacZ$^{fl/+}$* and *Sm22a^{Cre};R26-lacZ$^{fl/+}$* mice. To prove that these observations are not just limited to *Amhr2* and *Sm22a* reporter mice, we analyzed three additional mouse models: *Cspg4^{Cre};R26-lacZ$^{fl/+}$*, *Thy1^{Cre};lacZ$^{fl/+}$*, and *Acta1^{Cre};lacZ$^{fl/+}$*. We chose these promoters because they are broadly expressed in mesenchymal cells during embryonic development, but their expression is limited to specific mesenchymal cells postnatally, such as, CSPG4 in pericytes and ACTA1 in heart and skeletal muscles (Smith et al., 2019). Because, reporter expression is not inducible in these models, the presence of reporter-labeled epithelial cells

can be attributed to the mesoepithelial nature of the MDs rather than to MET. Therefore, we used *Cspg4*^{CreER}*;R26-lacZ*$^{fl/+}$ and *Pdgfrβ*^{rtTa}*;tetO*^{Cre}*;R26-lacZ*$^{fl/+}$ mice to be able to induce reporter expression at different stages of development and, thereby, investigate the contributions of embryonic and adult mesenchymal cells separately. Furthermore, we used an alternative strategy of labeling epithelial cells in *Pax8*^{rtTa}*;tetO*^{Cre}*;R26-lacZ*$^{fl/+}$ mice, and investigated whether the labeled epithelial cells are replaced by unlabeled mesenchymal cells over time. We also developed organoids from these mouse models to test the contribution of any rare mesenchymal cells that might have been missed during our *in vivo* studies. Using these methodologies, we found no strong evidence supporting the role of MET in the adult oviduct and uterus during homeostasis and regeneration.

RESULTS

Amhr2Cre-Driven, LacZ-Labeled Cells Are Present in the Epithelium by Birth

During embryonic development, coelomic epithelium invaginates to form the Müllerian duct epithelium (MDE) (Guioli et al., 2007; Orvis and Behringer, 2007). Initially, MDE is mesoepithelial in nature. Eventually, it progressively acquires epithelial features and differentiates into the epithelium of MD-derived organs. The surrounding mesenchymal cells, Müllerian duct mesenchyme (MDM), also progressively differentiates to acquire FRT organ-specific features of stroma and muscularis layers. Immunostaining for different mesenchymal markers, such as vimentin, platelet-derived growth factor receptor beta (PDGFRβ), αSMA, and an epithelial marker cytokeratin 8 (CK8) on adult mouse oviduct and uterus showed that the expression of these mesenchymal markers is limited to stroma and muscularis layer, and CK8 is expressed only in the epithelium (Figures 1A and 1B), suggesting that by adulthood, epithelial and mesenchymal cells are fully differentiated and express their respective markers. *Amhr2* expression is present in the coelomic epithelium and MDM (Baarends et al., 1994; Teixeira et al., 1996). To determine the fate of AMHR2^{+} cells, we developed *Amhr2*^{Cre}*;R26-lacZ*$^{fl/+}$ mice in which *lacZ*-encoded β-galactosidase expression is specific to AMHR2^{+} cells and their progenies (Figure 1C). Gross examination of reproductive tracts at postnatal day 1 (PND1) from these mice showed X-gal staining in FRT (Figure 1C). Histological examination revealed the presence of X-gal-stained cells in both stroma and epithelium of the oviduct and uterus (Figures 1D and S1A-S1E). Quantification of X-gal staining in oviduct showed increased labeling with time, suggesting that the *Amhr2*-driven, *lacZ*-labeled epithelial cells actively contribute to oviduct development and are not vestigial cells (Figure 1E). Using RNA *in situ* hybridization, we confirmed that the endogenous expression of *Amhr2* is limited to coelomic epithelium, MDM, and oviduct stroma (Figure 1F). We used adult mouse ovaries as a positive control in which *Amhr2* expression was limited to stromal cells and ovarian surface epithelium (Figure 1Fa). We also examined the endogenous *Amhr2* expression using *Amhr2-lacZ* mice in which *lacZ* expression is knocked into the *Amhr2* gene and is directly under the control of *Amhr2* promoter (Arango et al., 2008). Grossly, X-gal staining was present in the ovary, oviduct, and uterus (Figure 1Ga). Consistent with *Amhr2 mRNA* expression data, histological analyses confirmed that *Amhr2*-specific lacZ is expressed in adult FRT stroma but not in the epithelium (Figures 1Gb-d, S1F, and S1G). Collectively, these data showed the presence of *Amhr2Cre*-derived, lacZ-labeled cells in the epithelium of neonatal and adult

FRT and the absence of *Amhr2* mRNA and *Amhr2*-driven marker expression in adult FRT epithelium .

Cspg4Cre-Driven, LacZ-Labeled Cells Are Present in the FRT Epithelium

To confirm further our results in a different model system, we marked and traced the fate of chondroitin sulfate proteoglycan 4 (CSPG4)-expressing cells. During early embryonic development, CSPG4 is broadly expressed in mesenchymal cells, and later on, its expression is limited to a subset of mesenchymal cells known as pericytes (Smith et al., 2019). Therefore, we developed a mouse model in which *lacZ* expression is under the control of *Cspg4* promoter-driven Cre. Grossly, X-gal staining was present in the MD (E14) and the FRT at PND1 and adult stages (Figure 2A). Postnatal expression of CSPG4 is limited to perivascular cells (Figure 2B), but histological analyses of $Cspg4^{Cre};R26\text{-}lacZ^{fl/+}$ neonatal FTs revealed the presence of *Cspg4Cre*-driven, lacZ-labeled cells in both the epithelial and mesenchymal compartments (Figure 2Ca). Importantly, these labeled epithelial cells persisted in adulthood, and their number increased with age (Figures 2Cb and c and 2D). Moreover, immunostaining revealed that these *lacZ*-labeled epithelia consisted of both secretory ($PAX8^+$) and ciliated (Ac-TUB^+) cells (Figure 2E, arrowheads). To investigate whether these labeled cells survive pregnancy-induced remodeling, we collected $Cspg4^{Cre};R26\text{-}lacZ^{fl/+}$ mice FRTs after three consecutive pregnancies and found $lacZ^+$ epithelial cells in the oviducts even after three cycles of pregnancy and involution (Figures 2F-2H). Immunostaining confirmed that, similar to non-labeled cells, $lacZ^+$ cells also express estrogen receptor α (ERα) and respond to tamoxifen treatment, an estrogen agonist (Figures 2Ge and 2I-2K). Next, we isolated epithelium from $Cspg4^{Cre};R26\text{-}lacZ^{fl/+}$ mice oviducts and demonstrated that both labeled and non-labeled epithelial cells can contribute to organoid development (Figures 2L and 2M).

Similar to FTs, gross analysis of X-gal stained $Cspg4^{Cre};R26\text{-}lacZ^{fl/+}$ uteri showed *lacZ* expression in uterine stroma and blood vessels, and the expression was absent in littermate controls (Figure 3A). To screen extensively for any rare $lacZ^+$ cells, whole uterine arms of both control and mutant mice were cut into a series of 125-μm-thick sections and then analyzed (Figure 3B). No staining was observed in any of the control mice (Figure 3Ba). However, patches of $lacZ^+$ cells were present in the epithelium of some uterine sections at PND35 (Figures 3B and 3C). These labeled cells were present in both uterine luminal and glandular epithelial cells and showed no regional bias toward any specific anatomical location (Figure 3C). To ensure that the *lacZ* labeling is not because of CSPG4 expression in the uterine epithelium, we performed immunostaining for CSPG4 in X-gal stained neonatal (Figure 3Da-d) and adult nulliparous (Figure 3De and f) $Cspg4^{Cre};R26\text{-}lacZ^{fl/+}$ uteri. At both these stages, CSPG4 expression was restricted to the perivascular cells (Figure 3D). Contrary to our findings, previous reports have suggested that mesenchymal *Cre*-driven lacZ labeling appears in FRT epithelium only during post-injury and postpartum repair and regeneration (Huang et al., 2012; Patterson et al., 2013; Yin et al., 2019). This suggests that extensive remodeling and regeneration of epithelium during postpartum repair might allow for easier visualization of these labeled cells; otherwise, the mesenchymal Cre-derived $lacZ^+$ cells are also present in the FRTs of neonatal and nulliparous mice (Figures 1, 2, and 3). Tamoxifen treatment causes massive expansion of endometrial epithelium. Therefore, we

injected adult *Cspg4*^{Cre}*;R26-lacZ*$^{fl/+}$ mice with this drug to cause expansion of rarely labeled epithelial cells for easy visualization (Figure 3E). Both whole mount and histological sections revealed the presence of labeled cells in the uterine epithelium (Figures 3F-3I). Overall, these data demonstrate the presence of embryonic mesenchymal-specific, *Cre*-derived *lacZ*$^{+}$ epithelium in postnatal oviduct and uterus.

Smooth Muscle Protein 22-Alpha Cre (Sm22α^{Cre}), Thy1^{Cre}, and Actin Alpha 1 Skeletal Muscle-Cre (Acta1^{Cre})-Derived Labeled Cells Are Present in the FRT Epithelium

Consistent with the mesoepithelial nature of the MDE (Fritsch et al., 2013; Orvis and Behringer, 2007; Paranko and Virtanen, 1986), we observed the expression of vimentin but not CK8 in the undifferentiated MDE at the embryonic day 14.5 (E14.5; Figure S2A). Some MDE cells also expressed αSMA (Figure S2A). These data suggest that embryonically active mesenchymal marker-specific Cre can cause recombination in the MDE cells resulting in the labeling of epithelial cells. Therefore, we sought to examine the pattern of mesenchyme-specific *Cre*-driven *lacZ* expression in the Mouse Genome Informatics (MGI) database (Smith et al., 2019). Data relating to the FRT organs from a total of three mouse models *Sm22a*^{Cre}*; lacZ*$^{fl/+}$ (Boucher et al., 2003; Zhang et al., 2006), *Thy1*^{Cre}*;lacZ*$^{fl/+}$ (Dewachter et al., 2002), and *Acta1*^{Cre}*;lacZ*$^{fl/+}$ (Miniou et al., 1999) were available in this database, each reporting a distinct mesenchyme-specific marker-driven reporter expression profile in the FRT. SM22a, THY1, and ACTA1 are bona fide markers of mesenchymal cells and are not expected to be present in epithelial cells. A recent study has reported that *Sm22α*^{Cre}-derived cells are only present in the stromal compartment of nulliparous uterus and that these cells transition to the epithelium for postpartum repair and regeneration (Yin et al., 2019), suggesting that a population of stromal stem cells contribute directly to the uterine epithelial regeneration. In contrast, our MGI database search revealed that *Sm22α*^{Cre}-derived, *lacZ*-labeled cells are present in the FT and uterine epithelium of both pre-pubertal and adult *Sm22a*^{Cre}*; lacZ*$^{fl/+}$ mice (Figures S2B-S2I). A similar expression pattern was also observed in the two other mouse models: *Thy1*^{Cre}*;lacZ*$^{fl/+}$ and *Acta1*^{Cre}*;lacZ*$^{fl/+}$ (Figures S3A and S3B). Collectively, these observations suggest that the presence of mesenchyme-specific, *Cre*-driven labeling in the FRT epithelial cells, as reported by earlier studies, is possibly a result of the recombination occurring in the MDE itself because of its mesoepithelial nature.

Induction of *Cspg4Cre*-Driven Recombination after MD Development and in Adult FRT Does Not Label Epithelial Cells

To label cells after MD development is completed at E14 (Orvis and Behringer, 2007), we developed a *Cspg4*^{CreER}*;R26-lacZ*$^{fl/+}$ mouse model in which lacZ expression is under the control of tamoxifen-inducible *Cspg4* promoter-driven Cre. Time-mated, pregnant *Cspg4*^{CreER}*;R26-lacZ*$^{fl/+}$ mice were injected with a single dose of tamoxifen at E15.5 to induce *Cspg4Cre*-driven *lacZ* labeling in the fetuses (Figure 4A). Subsequently, FRTs were collected postnatally at different chase points (Figures 4B-4E). Gross analysis of both prepubertal and adult FRTs revealed *lacZ* labeling in the tamoxifen-treated, but not the vehicle-treated, mutants (Figures 4B-4E). These *lacZ*-labeled cells were mainly present around blood vessels in both the oviduct and the uterus at different chase points (Figures 4B-4E). Importantly, histologic analyses revealed the lack of any *lacZ* labeling in the

epithelial cells of prepubertal or adult FRTs (Figures 4Cb and 4Eb). Instead, the expression was restricted to the stromal perivascular cells of these organs (Figures 4Cb and 4Eb, arrowheads). Control oviducts and uteri did not show any X-gal staining (Figures 4Ba, 4Ca, 4Dc, and 4Ea). To investigate whether the progenies of *Cspg4*-expressing cells contribute to epithelium postnatally, we administered tamoxifen in adult *Cspg4*^{CreER};*R26-lacZ*$^{fl/+}$ mice to induce labeling in CSPG4^{+} cells (Figure 4F). Interestingly, after more than a year of chase period, both gross and histologic analyses of mutant FRTs showed the lack of any *lacZ* expression in the oviductal or the uterine epithelium (Figures 4G and 4H). As expected, the *lacZ* expression was restricted to the stromal perivascular cells (Figure 4H). Overall, these results suggest that after MD development, neither CSPG4-expressing cells nor their progenies contribute to the FRT epithelium.

Cell Fate Mapping in FRT Using *Pdgfrβ* Promoter-Driven Cre Reporter Mice

The main caveat of *Cspg4*^{CreER};*R26-lacZ*$^{fl/+}$, a tamoxifen-driven mouse model, is the inability to label most of the mesenchymal cells because tamoxifen treatment can have unwanted dose-dependent consequences on FRT organs. Therefore, one can argue that the absence of any *lacZ*-labeled epithelial cells in adult *Cspg4*^{CreER};*R26-lacZ*$^{fl/+}$ mice (Figure 4) is because all CSPG4-expressing mesenchymal cells were not labeled during the tamoxifen pulse. To overcome that issue, we developed another mouse model in which *lacZ* expression is under the control of doxycycline-inducible *Pdgfrβ*–promoter-driven Cre (Figure 5). We chose PDGFRβ because it faithfully marks the stromal cells of the oviduct and uterus (Figure 1). To label the maximum number of PDGFRβ^{+} cells, doxycycline was continuously administered in drinking water to *Pdgfrβ*^{rtTa};*tetO*^{Cre};*R26-lacZ*$^{fl/+}$ mice from E8.5 to PND1 to encompass the period of MD development and differentiation (Figure 5A). Because PDGFRβ is also expressed in fat cells (Vishvanath et al., 2016), we used the ovarian fat pad as a positive control to check for the specificity of *Pdgfrβ* promoter-driven *lacZ* expression. Doxycycline administration resulted in the *lacZ* labeling of ovarian bursal fat pads in mutants but not in controls, thus confirming the specificity of this mouse model (Figure 5B). Gross analysis of mutant FRTs revealed the presence of labeled cells in the oviduct as well as in the uterus (Figure 5B, 5C, and 5Fa). Importantly, histologic analyses revealed the presence of *lacZ*$^{+}$ cells in the epithelia of these organs (Figure 5Db and 5Fb). Positive controls showed the presence of labeled cells in ovarian bursa and ovarian surface epithelium, which has a mesoepithelial character (Figure 5Da). Next, we isolated whole FT and uterine epithelium from doxycycline-induced *Pdgfrβ*^{rtTa};*tetO*^{Cre};*R26-lacZ*$^{fl/+}$ mice and developed organoids from these freshly isolated epithelial cells. X-gal staining of these organoids revealed the presence of both *lacZ*-labeled as well as unlabeled organoids that are morphologically similar (Figures 5D, 5E, 5G, and 5H). Collectively, these results further confirm that mesenchyme-specific, *Cre*-driven, *lacZ*-labeled epithelial cells appear because of embryonic activity of the Cre in MDE.

PDGFRβ^{+} Cell-Derived Progenies in Adult FRT Are Restricted to the Mesenchymal Compartment and Do Not Contribute to Epithelial Cell Lineages

To complement the embryonic lineage tracing data from *Pdgfrβ*^{rtTa};*tetO*^{Cre};*R26-lacZ*$^{fl/+}$ mice, we developed a *Pdgfrβ*^{rtTa};*tetO*^{H2BJGFP} mouse model in which doxycycline administration induces nuclear GFP expression exclusively in PDGFRβ^{+} cells (Figures 5I

and 5J). If PDGFRβ$^+$ cell-derived progeny contribute toward epithelial cell lineage maintenance, nuclear GFP expression will be present in both stromal and epithelial cells. Alternatively, nuclear GFP expression will be limited to stromal cells, suggesting the absence of any such contribution (Figure 5I). Therefore, we treated adult *Pdgfrβ^{rtTa};tetO^{H2BJGFP}* mice with doxycycline for 3 days to induce nuclear GFP expression in PDGFRβ$^+$ cells and collected FRTs immediately for further analysis. Gross examination of FRT organs revealed the presence of GFP expression in doxycycline-treated mutants but not in controls, and the expression was consistent across the length of oviducts (Figure 5J). Because we did not notice any differences in the labeling pattern between oviduct and uterus throughout this study using several different mouse models, here, we focused exclusively on oviducts. As expected, co-localization of GFP with CK8 (an epithelial marker), PAX8, and Ac-TUB revealed the expression of nuclear GFP specifically in stromal cells but not in the epithelial cells (Figure 5K). A recent study has reported *in vitro* conversion of stromal cells into epithelial cells (Yin et al., 2019). Therefore, we co-cultured oviductal stromal and epithelial cells isolated from adult *Pdgfrβ^{rtTa};tetO^{H2BJGFP}* mice in the presence of doxycycline in the culture media (Figure 5L). Live imaging of cell culture plates for 21 days did not show any GFP expression in oviduct epithelial organoids (Figure 5L). However, intense nuclear GFP expression was present in the stromal cells (Figure 5L). Furthermore, we isolated oviduct epithelial cells from adult *Pdgfrβ^{rtTa};tetO^{H2BJGFP}* mice and developed organoids in the absence of stromal cells (Figures 5M and 5N). During the period of 21 days in culture and exposure to a low dose of doxycycline, we never observed GFP expression in oviduct organoids (Figures 5M and 5N).

An alternative explanation to these results would be that the conversion of stromal cells to epithelial cells is a very slow process and occurs only in few cells. In such a model, stromal to epithelial conversion might escape detection in short-label-chase experiments as we did in *Pdgfrβ^{rtTa};tetO^{H2BJGFP}* mice. To rule out this possibility, we treated adult *Pdgfrβ^{rtTa};tetO^{Cre};R26-lacZ$^{fl/+}$* mice with doxycycline for 2 months to label the maximum number of PDGFRβ$^+$ cells and chased them for 1 year (Figure 6A). Histological analysis of the oviducts and uteri collected from 1-year-old mutant mice showed that labeled cells were restricted to the stromal compartment and were completely absent in the epithelium (Figures 6A-6C). Furthermore, we developed organoids from oviductal and uterine epithelial cells isolated from these mice and performed X-gal staining. No labeling was observed in either oviductal or uterine organoids (Figures 6B and 6Cb). Collectively, these data suggested that mesenchymal lineages do not contribute to adult oviductal and uterine epithelial cells.

PAX8$^+$ Cells Self-Renew and Maintain Epithelium during Homeostasis and Regeneration

To investigate further the possibility of transdifferentiation of non-epithelial lineages to epithelial cells, we used an alternative approach of labeling most of the adult oviductal epithelial cells, instead of the stromal cells, and chased their fate. For that, we used *Pax8^{rtTa};tetO^{Cre};R26-lacZ$^{fl/+}$* mice in which *lacZ* expression is under the control of the doxycycline-inducible *Pax8* promoter (Figure 6D). PAX8 is a specific marker of human and mouse oviductal epithelial progenitor cells (Ghosh et al., 2017; Perets et al., 2013; Yamamoto et al., 2016). PAX8$^+$ cells self-renew and give rise to ciliated cells (Ghosh et al., 2017). If unlabeled stromal cells transdifferentiate into epithelial cells, one can expect a

progressive decline in the labeling index of epithelial cells over time (Figure 6D). Therefore, we induced epithelial cell labeling at saturation by treating *Pax8*^{rtTa};*tetO*^{Cre};*R26-lacZ*$^{fl/+}$ mice with doxycycline for 2 weeks (Figure 6D). Histological examination of the oviducts collected at 210 days after label induction, revealed an increase in the number of *lacZ*$^{+}$ epithelial cells in distal oviducts in which Pax8^{+}-cell-derived progenies progressively give rise to ciliated cells. However, the number of *lacZ*$^{+}$ epithelial cells remains unchanged in the proximal oviduct, which mainly consists of Pax8^{+} secretory cells (Figures 6E and 6F). Furthermore, we chased the fate of these initially labeled epithelial cells across multiple pregnancies because pregnancy is associated with extensive degeneration and regeneration of cells in the FRT (Figure 6G). Interestingly, even with this chase, the percentage of *lacZ*-labeled oviductal epithelial cells either increased or remained stable over time (Figures 6H and 6I). We have also performed similar pulse-chase experiments in the uterine epithelium and found that the labeling index of uterine epithelial cells also remains stable over longer chases (Syed et al., 2020). These results further confirm that, in adult oviduct and uterus, stromal cells are unlikely to contribute to epithelial cell lineages during homeostasis or regeneration.

DISCUSSION

FRT consists of tubal organs, such as FTs and uterus, and provides a site for fertilization and subsequent embryonic and fetal development. Normal functioning of these organs is essential for female fertility, and defects in their development and/or functions are associated with many human diseases (Teixeira et al., 2001), including high-grade serous ovarian cancer, the deadliest gynecological cancer. Histopathological analysis of FTs collected from *BRCA1/2* mutation-carrier patients undergoing risk-reducing salpingo-oophorectomy revealed the presence of ovarian cancer precursor lesions consisting of proliferating secretory cells in the tubes (Carcangiu et al., 2004; Medeiros et al., 2006; Piek et al., 2001) and suggesting that FT is a possible site of origin for serous ovarian cancer. Follow-up studies in mouse models targeting oncogenic mutations in the secretory cells of oviducts using *Pax8* or *Ovgp1* promoter provided experimental evidence that transformed secretory cells give rise to serous ovarian cancer (Perets et al., 2013; Sherman-Baust et al., 2014). Cell lineage tracing in mouse models and in *in vitro* analysis of human FT epithelial cells established that Pax8^{+} secretory cells act as stem/progenitor cells and give rise to ciliated cells through the modulation of the Wnt pathway (Ghosh et al., 2017; Yamamoto et al., 2016). Collectively, these studies firmly established that oncogenic transformation of PAX8^{+} epithelial cells lead to the development of serous ovarian cancer. In contrast, a study described that the deletion of *Dicer* and *Pten* in AMHR2^{+} oviductal stromal cells results in the development of serous ovarian cancer, suggesting the mesenchymal origin of these epithelial cancers (Hua et al., 2016; Kim et al., 2012). Here, we performed cell-lineage-tracing analysis of oviductal stromal and epithelial cells and showed that mesenchymal cells do not transdifferentiate to epithelial cells and that the oviductal epithelium in adult mice is maintained by PAX8^{+} epithelial cells. During embryonic development, AMHR2 expression is first detected in coelomic epithelium, which is the precursor of the MDE (Zhan et al., 2006). Therefore, *Amhr2Cre* is expected to be expressed in the coelomic epithelium and, subsequently, in the MDE, resulting in the presence of *Amhr2Cre*-driven reporter-labeled

cells in the FRT epithelium. These findings suggest that it is the endogenous expression of Amhr2 in the coelomic epithelium, rather than the process of MET, that is responsible for the presence of *Amhr2Cre*-derived, labeled cells in the oviductal epithelium.

STAR★METHODS

LEAD CONTACT AND MATERIALS AVAILABILITY

Lead Contact—Further information and requests for resources and reagents should be directed to and will be fulfilled by the Lead Contact, Assoc. Prof. Pradeep Tanwar (Pradeep.tanwar@newcastle.edu.au).

Materials Availability—All unique/stable reagents generated in this study are available from the Lead Contact with a completed Materials Transfer Agreement.

Data and Code Availability—Quantitative data supporting the figures is described in the paper. Additional data files will be made available upon reasonable request from the corresponding author.

EXPERIMENTAL MODEL AND SUBJECT DETAILS

Mice—All mice used in this study were maintained on the mixed genetic background (C57BL/6J; 129SvEv) and were housed under the standard housing conditions with *ad libitum* access to food and water. All animal procedures and experiments were approved by the Animal Care and Ethics Committee of the University of Newcastle, Australia. The parental mice strains $Amhr2^{tm3(cre)Bhr}$ (Jamin et al., 2002), $Amhr2^{tm2(lacZ)Bhr}$ (Arango et al., 2008), $Cspg4^{cre}$ (Zhu et al., 2008), $Cspg4^{CreER}$ (Zhu et al., 2011), $Pdgfrb^{rtTA}$ (Vishvanath et al., 2016), $Pax8^{rtTA}$ (Traykova-Brauch et al., 2008), $tetO^{Cre}$ (Perl et al., 2002), $tetO^{H2BJGFP}$ (Tumbar et al., 2004), $R26\text{-}lacZ^{fl/fl}$ (Soriano, 1999) were used in subsequent crosses to generate multiple transgenic mouse lines. $Amhr2^{tm3(cre)Bhr}$ and $Amhr2^{tm2(lacZ)Bhr}$ are hereafter referred to as $Amhr2^{Cre}$ and *Amhr2-lacZ*, respectively. $Pax8^{rtTA};tetO^{Cre}$ and $Pdgfrb^{rtTA};tetO^{Cre}$ double mutant mice were generated as a parental line by direct crossing of $Pax8^{rtTA}$ and $Pdgfrb^{rtTA}$ with $tetO^{Cre}$ mice for subsequent breeding with reporter lines to generate doxycycline regulated mouse models. To induce expression of lacZ-encoded β-galactosidase in Müllerian duct mesenchyme (MDE) for its genetic labeling, we crossed $Amhr2^{Cre}$, $Cspg4^{Cre}$ and $Cspg4^{CreER}$ mice with $R26\text{-}lacZ^{fl/fl}$ mice to generate $Amhr2^{Cre};R26\text{-}lacZ^{fl/+}$, $Cspg4^{Cre};R26\text{-}lacZ^{fl/+}$ and $Cspg4^{CreER};R26\text{-}lacZ^{fl/+}$ mice, respectively. $Pdgfrb^{rtTA}$ mice were crossed with $tetO^{H2BJGFP}$ mice to generate $Pdgfrb^{rtTA};tetO^{H2BJGFP}$ mice, which express human histone 1, H2BJ, protein (HIST1H2BJ) and Green Fluorescent Protein (GFP) fusion protein (referred to as H2BJGFP) transiently in Pdgfrβ-expressing cells. $Pdgfrb^{rtTA};tetO^{Cre}$ and $Pax8^{rtTA};tetO^{Cre}$ mice were crossed with $R26\text{-}lacZ^{fl/fl}$ mice to generate $Pdgfrb^{rtTA};tetO^{Cre};R26\text{-}lacZ^{fl/+}$ and $Pax8^{rtTA};tetO^{Cre};R26\text{-}lacZ^{fl/+}$ mice, respectively. Analysis of lacZ positive cells in the female reproductive organs of three mouse models $Sm22a^{Cre};lacZ^{fl/+}$ (Zhang et al., 2006), $Thy1^{Cre};lacZ^{fl/+}$ (Dewachter et al., 2002) and $Acta1^{Cre};lacZ^{fl/+}$ (Miniou et al., 1999) was done using publicly available Mouse Genome Informatics database.

To determine embryonic age, the day of vaginal plug detection was considered as embryonic day 0.5 (E0.5) and the day of birth was considered as postnatal day 1 (PND1). For gross analyses, whole tissue images were taken by Nikon SMZ25 microscope with an attached Nikon DS-Fi2 camera.

Cell lines—Wnt-3A, R-spondin3 and noggin expressing cell line L-WRN was purchased from ATCC and was used to produce WNT3A-RSPO3-NOGGIN conditioned medium (Miyoshi and Stappenbeck, 2013).

Oviductal organoids—Oviducts from adult female mice were collected for epithelial isolation. Briefly, both oviducts were placed on a clean Petri dish containing Dulbecco phosphate buffer saline (DPBS) to remove any excess vascular and connective tissues. The oviducts were then uncoiled under stereo microscope and microdissecetd into 1-2 mm small pieces and digested in enzyme solution (10 mg/ml Pronase from Streptomyces griseus (Sigma-Aldrich) and 0.5 mg/ml DNase I (Sigma-Aldrich) at 4°C for 13-14 hours. Enzymatic digestion was stopped by adding 10% v/v fetal bovine serum (FBS) (Bovogen) in the enzyme solution and the epithelium was then squeezed out from the oviductal pieces by using fine needles under stereo microscope. Isolated epithelial tubes were collected in the collection tube and a single cell suspension was prepared by repeated pipetting. These epithelial cells were then washed twice with DMEM-F12 media containing 5% FBS, 1% L-glutamine (HyClone) and 1% penicillin-streptomycin (Thermo Fisher Scientific). After washing, differential attachment was performed by incubating cells in a 10 cm cell culture plate containing the above mentioned DMEM-F12 media in an incubator at 37°C with 5% CO2. After 2 hours of incubation, media was collected in a 15 mL tube and centrifuged at 1500 rpm for 5 minutes to pellet the epithelial cells. The epithelial cell pellet was resuspended in 30% media and 70% Matrigel and was placed as 50 µl droplets in each well of a 24-well cell culture plate. The Matrigel with cells was allowed to solidify by at 37°C for 20 minutes. Each well of the culture plate was overlaid with 75% oviductal epithelial (ode) culture media (Dulbecco's modification of Eagle's medium/Ham's F-12 50/50 mix media (DMEM-Ham's F12) without L-glutamine (Mediatech, cat. no. 15-090), supplemented with 2% Ultroser G serum substitute (USG; Pall Corporation), 1% penicillin-streptomycin (Thermo Fisher Scientific) and 25% WNT3A-RSPO3-NOGGIN conditioned media (WRN-CM). WRN-CM was prepared from L-WRN cells (ATCC® CRL-3276) by following previously described protocol (Miyoshi and Stappenbeck, 2013). This media was further supplemented with several signaling modulators and growth factors, such as mouse epidermal growth factor (EGF; 100 ng/ml; Sigma-Aldrich), fibroblast growth factor 10 (FGF 10, 100ng/ml; Peprotech), nicotinamide (1mM; Sigma) and TGFBR1 kinase inhibitor IV (SB-431542; 0.5 µM; Selleckchem). ROCK inhibitor (Y-27632; 10 µM; TOCRIS) was added to the media only during the first 3 days of culture and passaging. Media was changed every 3 days. After 21 days in culture, organoids were harvested for further processing. During organoid development the images were captured by JuLi™ Stage Real-Time Cell History Recorder (NanoEnTek).

Uterine epithelial organoids—The uteri collected from adult female mice were washed with Mg^{2+} and Ca^{2+} free Hank's Balanced Salt Solution (HBSS). Uterine epithelium was

isolated as described previously (Syed et al., 2020). Briefly, uterine arm was slit open and cut longitudinally into 3-4 mm pieces. The tissue fragments were then incubated in Pronase/DNase enzyme solution [10mg/ml Pronase (Sigma-Aldrich) from *Streptomyces griseus* and 0.5 mg/ml DNase I (Sigma-Aldrich)] at 4°C on a shaker for 13-14 hours. Enzymatic digestion was stopped by adding 10% v/v fetal bovine serum (FBS) (Bovogen), and uterine epithelium was collected after passing through 70 μm cell strainer. Cells were then washed with DMEM-F12 media containing 5% FBS, 1% L-glutamine (Sigma-Aldrich) and 1% penicillin-streptomycin (Thermo Fisher Scientific) by centrifugation at 1500 rpm for 5 minutes. After washing cells were incubated for 2 hours in a cell culture plate with above-mentioned FBS containing DMEM-F12 media for differential attachment.

After differential attachment, uterine epithelial cells were resuspended in 30% media and 70% matrigel and was placed as 50 μl droplets in each well of a 24-well cell culture plate. Matrigel droplets were incubated at 37°C for 20 minutes for solidification and were then overlaid with uterine organoid culture medium as described previously (Syed et al., 2020). The uterine organoid culture medium contained 25% Wnt3A-R-spondin3-noggin conditioned media (WRN-CM) and 75% DMEM-F12, supplemented with 1% Glutamax (Thermo Fisher Scientific), 1% penicillin-streptomycin (Thermo Fisher Scientific) and additional growth factors such as 2% B27 (Thermo Fisher Scientific), 1% N2 (Thermo Fisher Scientific), 1% insulin-transferrin-selenium (ITS) (Sigma-Aldrich), 50 ng/ml mouse EGF (Sigma-Aldrich), 50ng/ml human FGF10 (Peprotech), 1mM nicotinamide (Sigma-Aldrich), 0.5 μM A83-01 (TGFβ/Alk inhibitor) (Tocris) and 10 μM Y-27632 dihydrochloride (Rock inhibitor) (Tocris). ROCK inhibitor (Y-27632; 10 μM; TOCRIS) was only added to the media during the first 3 days of culture. Media was changed every 3-4 days and after 12 days organoids were harvested for further processing.

METHOD DETAILS

Embryonic and adult cell lineage tracing experiments—For embryonic labeling of the Müllerian duct mesenchyme with lacZ in $Cspg4^{CreER};R26\text{-}lacZ^{fl/+}$ mice, pregnant $R26\text{-}lacZ^{fl/fl}$ females mated with $Cspg4^{CreER}$ males were administered with a single intraperitoneal tamoxifen injection (40 mg/kg B.W. in sesame oil at a concentration of 20 mg/ml) at gestation day 15.5 (equivalent to E15.5). Female reproductive tracts from these tamoxifen exposed pups were collected at postnatal day 14 (PND14) and 56 (PND56). For embryonic induction of lacZ-encoded β-galactosidase in $Pdgfrb^{rtTA};tetO^{Cre};R26\text{-}lacZ^{fl/+}$ mice, pregnant females were administered with 5 mg/ml doxycycline (Sigma) in drinking water (supplemented with 1% sucrose) from embryonic day 8.5 (E8.5) to postnatal day 1 (PND1). Female reproductive tracts were dissected out and tissues collected at 12 months age.

For adult labeling in $Cspg4^{CreER};R26\text{-}lacZ^{fl/+}$ mice, 10mg of tamoxifen was administered by intraperitoneal injection (five injections of 2 mg each; every 24 hours) to 5-7 weeks old female mice, along with three subcutaneous injections of progesterone (1mg each; every 48 hours). Furthermore, for induction of lacZ-encoded β-galactosidase in adult $Pdgfrb^{rtTA};tetO^{Cre};R26\text{-}lacZ^{fl/+}$ and $Pax8^{rtTA};tetO^{Cre};R26\text{-}lacZ^{fl/+}$ female mice, 5 mg/ml doxycycline (Sigma) was administered in drinking water (supplemented with 5% sucrose) at

6-8 weeks of age for two months or two weeks duration, respectively. Female reproductive tracts from *Pdgfrb*^{rtTA};*tetO*^{Cre};*R26-lacZ*$^{fl/+}$ mice were collected 12 months post-induction and from *Pax8*^{rtTA};*tetO*^{Cre};*R26-lacZ*$^{fl/+}$ mice at 7 months post-induction. To induce GFP expression in *Pdgfrb*^{rtTA};*tetO*^{H2BJGFP} female mice, 5 mg/ml doxycycline was given in drinking water (supplemented with 5% sucrose) for two days in 6-8 weeks old mice. Female reproductive tracts were collected 24 hours later to visualize GFP expression.

Doxycycline treatment to induce GFP expression in oviductal organoids— *Pdgfrb*^{rtTA};*tetO*^{H2BJGFP} female mice express H2BJGFP in PDGFRβ-expressing cells specifically. However, *tetO*^{H2BJGFP} expression is terminated upon withdrawal of doxycycline, such that with each cell division the label intensity is diluted to half. Thus, for continuous GFP expression in PDGFRβ-expressing cells, we added and maintained 1 mg/ml doxycycline in oviductal organoid culture medium during the whole 21-day culture period. For the co-culture of oviductal organoids with PDGFRβ-expressing stromal fibroblasts, native GFP fluorescence images were taken using JuLi™ Stage Real-Time Cell History Recorder (NanoEnTek) every 3 days.

Tamoxifen treatment—To investigate the effect of tamoxifen administration on lineage labeled cells, 10mg of tamoxifen (Sigma, diluted in sesame oil) was administered by intraperitoneal injection (five injections of 2mg each; every 24 hours) to 5-6 weeks old *Cspg4*^{CreER};*R26-lacZ*$^{fl/fl}$ female mice, and tissues were collected one week after the last tamoxifen injection.

RNA *in situ* hybridization—Müllerian ducts and adult mouse oviducts were collected at E15.5 and PND28, respectively, for RNA *in situ* hybridization. Briefly, the tissues were fixed in 10% buffered formalin for 24 hours at room temperature. Tissues were then embedded in paraffin and sectioned at 4μm thickness for further processing. RNA *in situ* hybridization was performed using RNAscope 2.5 High Definition Red Kit (Advanced Cell Diagnostics, Hayward, CA) as described (Goad et al., 2017).

X-gal/β-galactosidase staining—X-gal/β-galactosidase staining was performed by following previously described protocol (Tanwar et al., 2012). Briefly, intact MD and oviducts were pre-fixed in 4% paraformaldehyde at 4°C for 1 hour before washing with rinse buffer (0.1% sodium deoxycholate, 0.2% NP40, 2mM magnesium chloride in 0.1M phosphate) 3 times for 30 minutes each at room temperature. Tissues were incubated in X-gal (Bioline) solution post-washing for 8-10 hours at room temperature. X-gal/β-galactosidase stained, or unstained tissues were then fixed with 4% paraformaldehyde at 4°C overnight. For, whole mount imaging, uterine arms were sliced at 125 μm transverse sections using Mcllwain Tissue Chopper. Paraffin embedded tissue sections were cut at 5-8 μm thickness and processed for further immunostaining or nuclear fast red (Sigma) staining.

X-gal/β-galactosidase staining of organoids was also performed as described above, except for pre-fixation, which was done for 15 minutes at room temperature, and washing, which was done in rinse buffer without NP40. X-gal staining of Matrigel-embedded organoids was performed in 24-well cell culture plates to minimize the loss of organoids during the staining process.

Immunofluorescence (IF), immunohistochemistry (IHC) and nuclear fast (NF) staining—Tissues and organoids were fixed in 4% (w/v) paraformaldehyde at 4°C overnight, before processing for paraffin embedding and sectioning. For IF, IHC and nuclear fast staining, 6 μm thick tissue sections were deparaffinized followed by rehydration and processed separately according to respective protocols. For nuclear fast staining, rehydrated sections were incubated in nuclear fast red solution (Sigma) at room temperature for 4 minutes. Subsequently, the tissue sections were washed and dehydration for long term storage. For IF and IHC staining, antigen retrieval was done on rehydrated tissue sections by heating them at 98°C for 30 minutes in EDTA buffer (1mM; pH 8.0). After blocking, sections were incubated with primary antibodies at 4°C overnight. The primary antibodies used were rabbit anti-PAX8 (1:1000; catalog number 10336-1-AP; Proteintech), mouse anti-Acetylated-Tubulin (1:1000; catalog number T7451, clone 6-11B-1, Sigma-Aldrich), rabbit anti-β-galactosidase (1:250; catalog number A11132, Life Technologies), rabbit anti-ERα (1:750; catalog number sc-542, Santa Cruz Biotechnology), rabbit anti-PDGFRβ (1: 250; catalog number 3169, Cell Signaling Technology), rabbit anti-CSPG4 (1:200; catalog number AB5320, Millipore), rat anti-keratin 8 (1:250; catalog number TROMA-I, Developmental Studies Hybridoma Bank) and chicken anti-GFP (1:1000; catalog number Ab13970, Abcam). The secondary antibodies were Alexa 488/594 conjugated anti-rabbit/mouse/rat/chicken IgG (1:250; Jackson ImmunoResearch Labs) for IF and Biotin or HRP conjugated anti-rabbit/mouse IgG (1:250; Jackson ImmunoResearch Labs) for IHC.

Microscopy and image acquisition—Brightfield and fluorescence images were acquired using Olympus DP72 CCD (charge-coupled device) with color camera using cell-Sens software (Olympus) or Olympus BX43 fluorescence microscope with Olympus objectives (x4, NA = 0.16; x10, NA = 0.46; x20, NA = 0.75; x40, NA = 0.95). Olympus Fluoview FV10i upright confocal laser scanning microscope with 60x oil-immersion objective (NA = 1.35) (Olympus) and FV10i-SW software was used to acquire fluorescence images. Whole mount images of X-gal stained 125 μm thick sections and organoids were acquired by using SMZ25 stereoscope equipped with Nikon DS-Fi2 camera and Nikon P2-SHR Plan Apo 2X objective (NA = 0.312). Images consisted of 15–30 stacks with variable z-spacing and were captured and merged using NIS-Elements software. Organoid images during culture period were captured by JuLi™ Stage Real-Time Cell History Recorder (NanoEnTek). All imaging was done at room temperature except organoid imaging during the culture period was done at 37° C .

QUANTIFICATION AND STATISTICAL ANALYSIS

Image analysis and quantification was done using ImageJ software (NIH) and statistical analyses were performed on GraphPad Prism (v.7.04). Statistical analyses were done using two-way ANOVA and unpaired t test. Data are presented as mean ± SEM. P values less than 0.05 were considered as statistically significant.

Supplementary Material

Refer to Web version on PubMed Central for supplementary material.

ACKNOWLEDGMENTS

Work in the Tanwar lab was in part supported by funding from National Health and Medical Research Council, Cancer Australia, Ovarian Cancer Research Foundation, and the Dorothy Jean Cunningham Endometrial Cancer Research bequest. Teixeira lab was supported by NIH HDO72489.

REFERENCES

Arango NA, Kobayashi A, Wang Y, Jamin SP, Lee HH, Orvis GD, and Behringer RR (2008). A mesenchymal perspective of müllerian duct differentiation and regression in Amhr2-lacZ mice. Mol. Reprod. Dev 75, 1154–1162. [PubMed: 18213646]

Baarends WM, van Helmond MJ, Post M, van der Schoot PJ, Hooger-brugge JW, de Winter JP, Uilenbroek JT, Karels B, Wilming LG, Meijers JH, et al. (1994). A novel member of the transmembrane serine/threonine kinase receptor family is specifically expressed in the gonads and in mesenchymal cells adjacent to the müllerian duct. Development 120, 189–197. [PubMed: 8119126]

Boucher P, Gotthardt M, Li WP, Anderson RG, and Herz J (2003). LRP: role in vascular wall integrity and protection from atherosclerosis. Science 300, 329–332. [PubMed: 12690199]

Carcangiu ML, Radice P, Manoukian S, Spatti G, Gobbo M, Pensotti V, Crucianelli R, and Pasini B (2004). Atypical epithelial proliferation in fallopian tubes in prophylactic salpingo-oophorectomy specimens from BRCA1 and BRCA2 germline mutation carriers. Int. J. of Gynecol. Pathol 23, 35–40. [PubMed: 14668548]

Chari S, Nguyen A, Saxe J, and Sweet DJ (2017). Lineage tracing across 10 years. Cell Stem Cell 20, 733–734. [PubMed: 28575683]

Daikoku T, Hirota Y, Tranguch S, Joshi AR, DeMayo FJ, Lydon JP, Ellenson LH, and Dey SK (2008). Conditional loss of uterine Pten unfailingly and rapidly induces endometrial cancer in mice. Cancer Res. 68, 5619–5627. [PubMed: 18632614]

Daikoku T, Jackson L, Besnard V, Whitsett J, Ellenson LH, and Dey SK (2011). Cell-specific conditional deletion of Pten in the uterus results in differential phenotypes. Gynecol. Oncol 122, 424–429. [PubMed: 21570712]

Dewachter I, Reversé D, Caluwaerts N, Ris L, Kuipéri C, Van den Haute C, Spittaels K, Umans L, Serneels L, Thiry E, et al. (2002). Neuronal deficiency of presenilin 1 inhibits amyloid plaque formation and corrects hippocampal long-term potentiation but not a cognitive defect of amyloid precursor protein [V717I] transgenic mice. J. Neurosci 22, 3445–3453. [PubMed: 11978821]

Fritsch H, Hoermann R, Bitsche M, Pechriggl E, and Reich O (2013). Development of epithelial and mesenchymal regionalization of the human fetal utero-vaginal anlagen. J. Anat 222, 462–472. [PubMed: 23406280]

Ghosh A, Syed SM, and Tanwar PS (2017). *In vivo* genetic cell lineage tracing reveals that oviductal secretory cells self-renew and give rise to ciliated cells. Development 144, 3031–3041. [PubMed: 28743800]

Goad J, Ko YA, Kumar M, Syed SM, and Tanwar PS (2017). Differential Wnt signaling activity limits epithelial gland development to the anti-mesome-trial side of the mouse uterus. Dev. Biol 423, 138–151. [PubMed: 28153546]

Guioli S, Sekido R, and Lovell-Badge R (2007). The origin of the müllerian duct in chick and mouse. Dev. Biol 302, 389–398. [PubMed: 17070514]

Hua Y, Choi PW, Trachtenberg AJ, Ng AC, Kuo WP, Ng SK, Dinulescu DM, Matzuk MM, Berkowitz RS, and Ng SW (2016). Epithelialization of mouse ovarian tumor cells originating in the fallopian tube stroma. Oncotarget 7, 66077–66086. [PubMed: 27602775]

Huang CC, Orvis GD, Wang Y, and Behringer RR (2012). Stromal-to-epithelial transition during postpartum endometrial regeneration. PLoS ONE 7, e44285. [PubMed: 22970108]

Jamin SP, Arango NA, Mishina Y, Hanks MC, and Behringer RR (2002). Requirement of Bmpr1a for Müllerian duct regression during male sexual development. Nat. Genet 32, 408–410. [PubMed: 12368913]

Kim J, Coffey DM, Creighton CJ, Yu Z, Hawkins SM, and Matzuk MM (2012). High-grade serous ovarian cancer arises from fallopian tube in a mouse model. Proc. Natl. Acad. Sci. USA 109, 3921–3926. [PubMed: 22331912]

Kretzschmar K, and Watt FM (2012). Lineage tracing. Cell 148, 33–45. [PubMed: 22265400]

Medeiros F, Muto MG, Lee Y, Elvin JA, Callahan MJ, Feltmate C, Garber JE, Cramer DW, and Crum CP (2006). The tubal fimbria is a preferred site for early adenocarcinoma in women with familial ovarian cancer syndrome. Am. J. Surg. Pathol 30, 230–236. [PubMed: 16434898]

Miniou P, Tiziano D, Frugier T, Roblot N, Le Meur M, and Melki J (1999). Gene targeting restricted to mouse striated muscle lineage. Nucleic Acids Res. 27, e27. [PubMed: 10481039]

Miyoshi H, and Stappenbeck TS (2013). In vitro expansion and genetic modification of gastrointestinal stem cells in spheroid culture. Nat. Protoc 8, 2471–2482. [PubMed: 24232249]

Mullen RD, and Behringer RR (2014). Molecular genetics of müllerian duct formation, regression and differentiation. Sex Dev. 8, 281–296. [PubMed: 25033758]

Orvis GD, and Behringer RR (2007). Cellular mechanisms of müllerian duct formation in the mouse. Dev. Biol 306, 493–504. [PubMed: 17467685]

Owusu-Akyaw A, Krishnamoorthy K, Goldsmith LT, and Morelli SS (2019). The role of mesenchymal-epithelial transition in endometrial function. Hum. Reprod. Update 25, 114–133. [PubMed: 30407544]

Paranko J, and Virtanen I (1986). Epithelial and mesenchymal cell differentiation in the fetal rat genital ducts: changes in the expression of cytokeratin and vimentin type of intermediate filaments and desmosomal plaque proteins. Dev. Biol 177, 135–145.

Patterson AL, Zhang L, Arango NA, Teixeira J, and Pru JK (2013). Mesenchymal-to-epithelial transition contributes to endometrial regeneration following natural and artificial decidualization. Stem Cells Dev. 22, 964–974. [PubMed: 23216285]

Pei D, Shu X, Gassama-Diagne A, and Thiery JP (2019). Mesenchymal-epithelial transition in development and reprogramming. Nat. Cell Biol 21, 44–53. [PubMed: 30602762]

Perets R, Wyant GA, Muto KW, Bijron JG, Poole BB, Chin KT, Chen JY, Ohman AW, Stepule CD, Kwak S, et al. (2013). Transformation of the fallopian tube secretory epithelium leads to high-grade serous ovarian cancer in Brca;Tp53;Pten models. Cancer Cell 24, 751–765. [PubMed: 24332043]

Peri LE, Koh BH, Ward GK, Bayguinov Y, Hwang SJ, Gould TW, Mullan CJ, Sanders KM, and Ward SM (2015). A novel class of interstitial cells in the mouse and monkey female reproductive tracts. Biol. Reprod 92, 102. [PubMed: 25788664]

Perl AK, Wert SE, Nagy A, Lobe CG, and Whitsett JA (2002). Early restriction of peripheral and proximal cell lineages during formation of the lung. Proc. Natl. Acad. Sci. USA 99, 10482–10487. [PubMed: 12145322]

Piek JM, van Diest PJ, Zweemer RP, Jansen JW, Poort-Keesom RJ, Menko FH, Gille JJ, Jongsma AP, Pals G, Kenemans P, and Verheijen RH (2001). Dysplastic changes in prophylactically removed Fallopian tubes of women predisposed to developing ovarian cancer. J. Pathol 195, 451–456. [PubMed: 11745677]

Russo A, Czarnecki AA, Dean M, Modi DA, Lantvit DD, Hardy L, Baligod S, Davis DA, Wei JJ, and Burdette JE (2018). PTEN loss in the fallopian tube induces hyperplasia and ovarian tumor formation. Oncogene 37, 1976–1990. [PubMed: 29367766]

Schneider CA, Rasband WS, and Elicieri KW (2012). NIH Image to ImageJ: 25 years of image analysis. Nat. Methods 9, 671–675. [PubMed: 22930834]

Sherman-Baust CA, Kuhn E, Valle BL, Shih IeM., Kurman RJ, Wang TL, Amano T, Ko MS, Miyoshi I, Araki Y, et al. (2014). A genetically engineered ovarian cancer mouse model based on fallopian tube transformation mimics human high-grade serous carcinoma development. J. Pathol 233, 228–237. [PubMed: 24652535]

Smith CM, Hayamizu TF, Finger JH, Bello SM, McCright IJ, Xu J, Baldarelli RM, Beal JS, Campbell J, Corbani LE, et al. (2019). The mouse Gene Expression Database (GXD): 2019 update. Nucleic Acids Res. 47 (D1), D774–D779. [PubMed: 30335138]

Song IO, Hong SR, Huh Y, Yoo KJ, Koong MK, Jun JY, and Kang IS (1998). Expression of vimentin and cytokeratin in eutopic and ectopic endometrium of women with adenomyosis and ovarian endometrioma. Am. J. Reprod. Immunol 40, 26–31. [PubMed: 9689357]

Soriano P (1999). Generalized lacZ expression with the ROSA26 Cre reporter strain. Nat. Genet 21, 70–71. [PubMed: 9916792]

Syed SM, Kumar M, Ghosh A, Tomasetig F, Ali A, Whan RM, Alterman D, and Tanwar PS (2020). Endometrial axin2+ cells drive epithelial homeostasis, regeneration, and cancer following oncogenic transformation. Cell Stem Cell 26, 64–80.e13. [PubMed: 31883834]

Tanwar PS, Kaneko-Tarui T, Zhang L, Tanaka Y, Crum CP, and Teixeira JM (2012). Stromal liver kinase B1 [STK11] signaling loss induces oviductal adenomas and endometrial cancer by activating mammalian Target of Rapamycin Complex 1. PLoS Genet. 8, e1002906. [PubMed: 22916036]

Teixeira J, He WW, Shah PC, Morikawa N, Lee MM, Catlin EA, Hudson PL, Wing J, Maclaughlin DT, and Donahoe PK (1996). Developmental expression of a candidate müllerian inhibiting substance type II receptor. Endocrinology 137, 160–165. [PubMed: 8536608]

Teixeira J, Maheswaran S, and Donahoe PK (2001). Müllerian inhibiting substance: an instructive developmental hormone with diagnostic and possible therapeutic applications. Endocr. Rev 22, 657–674. [PubMed: 11588147]

Traykova-Brauch M, Schonig K, Greiner O, Miloud T, Jauch A, Bode M, Felsher DW, Glick AB, Kwiatkowski DJ, Bujard H, et al. (2008). An efficient and versatile system for acute and chronic modulation of renal tubular function in transgenic mice. Nat. Med 14, 979–984. [PubMed: 18724376]

Tumbar T, Gausch G, Greco V, Blanpain C, Lowry WE, Rendl M, and Fuchs E (2004). Defining the epithelial stem cell niche in skin. Science 303, 359–363. [PubMed: 14671312]

Vishvanath L, MacPherson KA, Hepler C, Wang QA, Shao M, Spurgin SB, Wang MY, Kusminski CM, Morley TS, and Gupta RK (2016). Pdgfrβ^{+} mural preadipocytes contribute to adipocyte hyperplasia induced by high-fat-diet feeding and prolonged cold exposure in adult mice. Cell Metab. 23, 350–359. [PubMed: 26626462]

Wu R, Zhai Y, Kuick R, Karnezis AN, Garcia P, Naseem A, Hu TC, Fearon ER, and Cho KR (2016). Impact of oviductal versus ovarian epithelial cell of origin on ovarian endometrioid carcinoma phenotype in the mouse. J. Pathol 240, 341–351. [PubMed: 27538791]

Yamamoto Y, Ning G, Howitt BE, Mehra K, Wu L, Wang X, Hong Y, Kern F, Wei TS, Zhang T, et al. (2016). In vitro and in vivo correlates of physiological and neoplastic human Fallopian tube stem cells. J. Pathol 238, 519–530. [PubMed: 26415052]

Yin M, Zhou HJ, Lin C, Long L, Yang X, Zhang H, Taylor H, and Min W (2019). $CD34^{+}KLF4^{+}$ stromal stem cells contribute to endometrial regeneration and repair. Cell Rep, 27, 2709–2724.e3. [PubMed: 31141693]

Zhan Y, Fujino A, MacLaughlin DT, Manganaro TF, Szotek PP, Arango NA, Teixeira J, and Donahoe PK (2006). Müllerian inhibiting substance regulates its receptor/SMAD signaling and causes mesenchymal transition of the coelomic epithelial cells early in Müllerian duct regression. Development 133, 2359–2369. [PubMed: 16687449]

Zhang J, Zhong W, Cui T, Yang M, Hu X, Xu K, Xie C, Xue C, Gibbons GH, Liu C, et al. (2006). Generation of an adult smooth muscle cell-targeted Cre recombinase mouse model. Arterioscler. Thromb. Vasc. Biol 26, e23–e24. [PubMed: 16484601]

Zhu X, Bergles DE, and Nishiyama A (2008). NG2 cells generate both oligodendrocytes and gray matter astrocytes. Development 135, 145–157. [PubMed: 18045844]

Zhu X, Hill RA, Dietrich D, Komitova M, Suzuki R, and Nishiyama A (2011). Age-dependent fate and lineage restriction of single NG2 cells. Development 138, 745–753. [PubMed: 21266410]

Highlights

- A subset of neonatal oviductal and uterine epithelial cells express mesenchymal markers
- Embryonic lineage tracing reveals their presence and expansion with age
- In adult organs, mesenchymal marker expression is limited to stromal cells
- Lineage tracing in adult mice provides no evidence of mesenchymal-epithelial transition

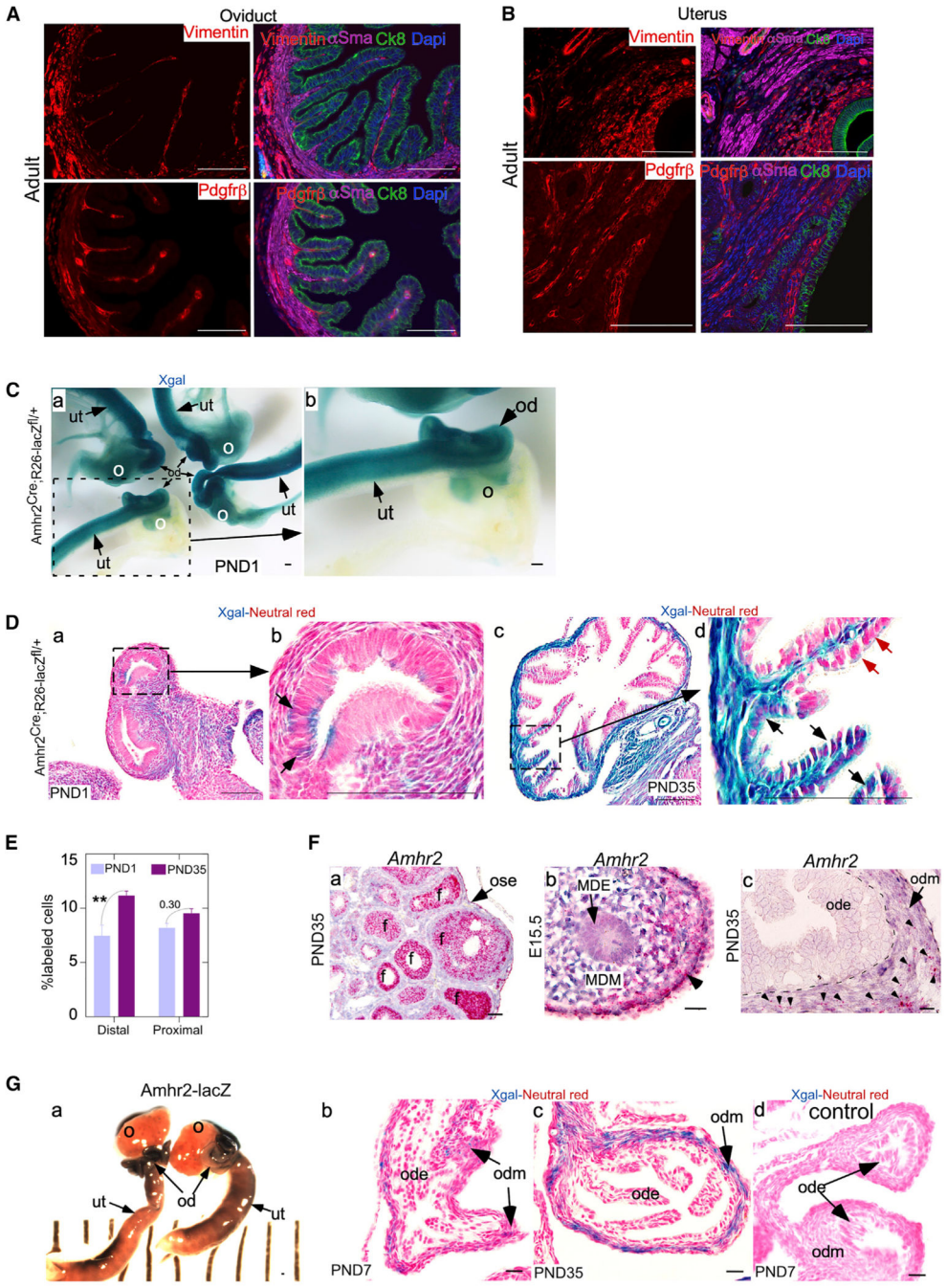

Figure 1. *Amhr2Cre*-Driven LacZ-Labeled Cells Are Present in Oviductal and Uterine Epithelium by Birth

(A) Immunostaining in adult mouse oviduct showing vimentin, αSMA, and PDGFRβ expression in stromal and muscularis layer and CK8 expression in the adjacent epithelium (n = 4 mice).

(B) Colocalization of vimentin, αSMA, PDGFRβ, and CK8 in adult mouse uterus (n = 4 mice).

(C) X-gal stained whole-mount images of *Amhr2*^{Cre}*;R26-lacZ*$^{fl/+}$ mouse neonatal oviduct and uterus (a and b). Subpanel b is the higher magnification of the inset in subpanel a.

(D) X-gal-stained tissue sections showing the presence of *lacZ*$^{+}$ cells in postnatal day 1 (PND1) (a and b) and PND35 oviductal epithelium (c and d). Subpanels b and d are higher magnifications of insets in a and c, respectively (PND1, n = 3 mice; PND35, n = 3 mice).
(E) Quantification of labeling index depicting an increase in the percentage of *lacZ*$^{+}$ cells in the PND35 oviduct epithelium compared with PND1 (PND1, n = 3 mice; PND35, n = 3 mice; **p = 0.0054; ^{ns}p = 0.3008).
(F) *In situ* hybridization for *Amhr2* mRNA (marked with red dots) in ovary (a), müllerian duct mesenchyme (b), coelomic epithelium (arrowhead, b) and adult oviductal stroma (arrowheads, c) (E15.5, n = 4 mice; PND35, n = 4 mice).
(G) X-gal staining of whole-mount oviducts (a) and the tissue sections (b and c) in *Amhr2-lacZ* mice at indicated chase points, showing real-time *lacZ* expression in stroma but not in epithelium, and the absence of *lacZ* expression in controls (d) (PND7, n = 4 mice; PND35, n = 4 mice).
Data represent means ± SEM; p values are indicated; two-way ANOVA with Sidak's test. Black and red arrows point to *lacZ*$^{+}$ and *lacZ*$^{-}$ epithelial cells, respectively, in (D). f, follicle; MD, müllerian duct; ut, uterus; od, oviduct; ode, oviductal epithelium; odm, oviductal mesenchyme; o, ovary; MDE, müllerian duct epithelium; MDM, müllerian duct mesenchyme. Scale bars, 100 μm.

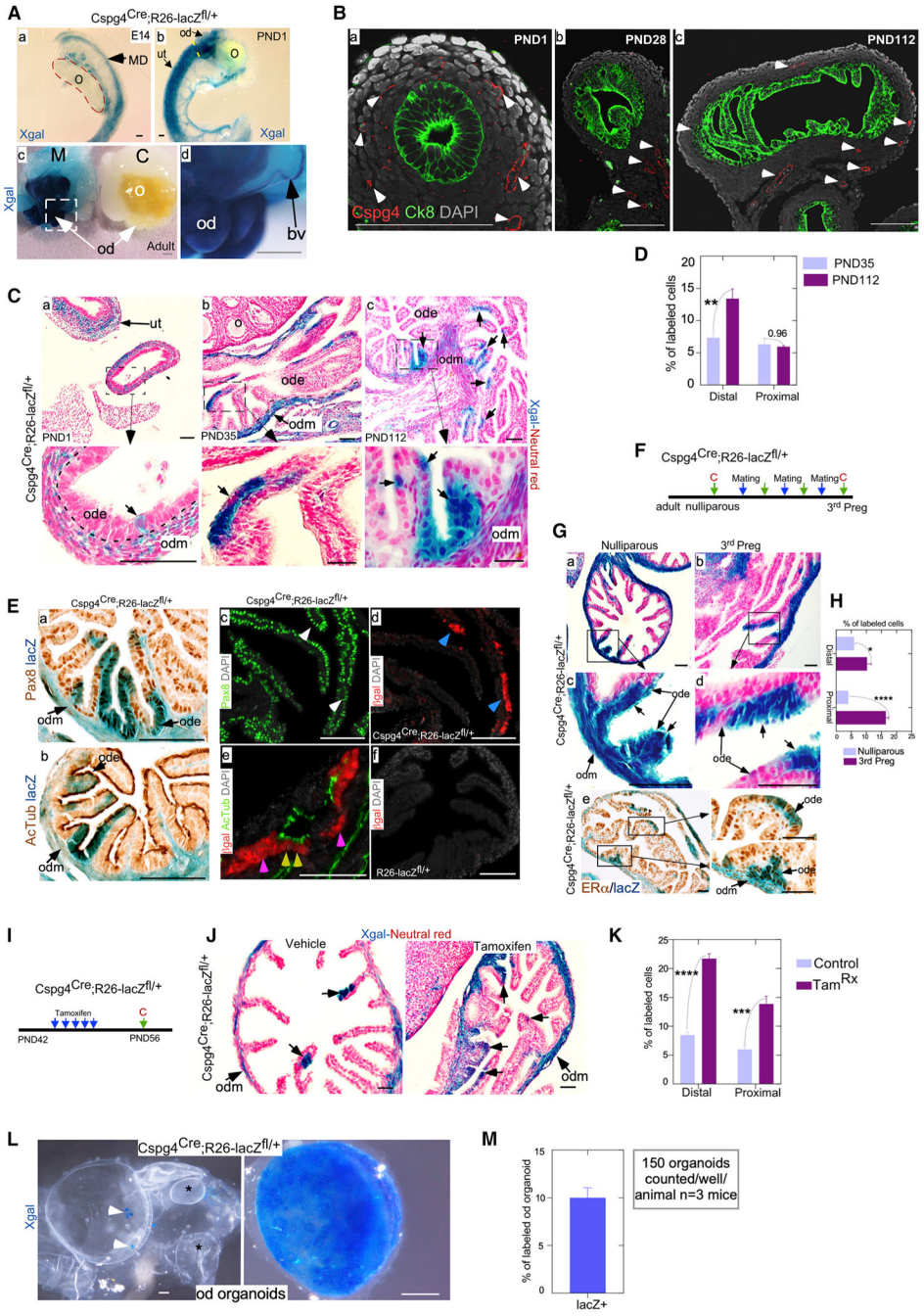

Figure 2. *Cspg4Cre*-Driven, LacZ-Labeled Cells Are Present in the Female Reproductive Tract Epithelium

(A) X-gal stained whole-mount images of *Cspg4^{Cre};R26-lacZ$^{fl/+}$* mouse MD (E14) (a), neonatal oviducts and uterus (b), and adult oviducts and ovaries (c and d), showing X-gal staining in mutants (M) but not in controls (C). Blood vessels were also positive for X-gal staining (d). (E14, n = 5 mice; PND1, n = 5 mice; adults, n = 5 mice).

(B) Co-immunostaining for CSPG4 and CK8 in postnatal day 1 (PND1) (a), PND28 (b), and PND112 (c) mouse oviducts showing CSPG4 expression in postnatal stromal perivascular

cells but not in $CK8^+$ epithelium (PND1, n = 3 mice; PND28, n = 3 mice; PND112, n = 3 mice).

(C) Representative histological images of X-gal-stained *Cspg4^{Cre};R26-lacZ$^{fl/+}$* mouse oviducts showing the presence of $lacZ^+$ cells in PND1 (a), PND35 (b), and PND112 (c) epithelium. (PND1, n = 5 mice; PND35, n = 4 mice; PND112, n = 4 mice).

(D) Quantification for *lacZ* labeled epithelium in distal and proximal oviduct at PND35 and PND112 (PND35, n = 4 mice; PND112, n = 4 mice; **p = 0.0025; ^{ns}p = 0.9615).

(E) Immunostaining for PAX8 (a secretory cell marker) and Ac-TUB (a ciliated cell marker) in tissue sections of PND35 (a and b) and PND112 (c–f) mouse oviducts showing that *lacZ$^+$* epithelial cells are both secretory and ciliated in nature. Subpanel c and d are serial sections of the same tissue. Control oviduct from *R26-lacZ$^{fl/+}$* mouse depicted no βgal staining (f). (PND35, n = 4 mice; PND112, n = 4 mice).

(F) Experimental schedule used in (G) to track the fate of labeled epithelial cells across multiple pregnancies.

(G) Representative histological images of mouse oviducts stained with X-gal alone (a–d) or in combination with immunostaining for estrogen receptor α (ERα) (e), showing that *lacZ$^+$* epithelial cells persist during multiple pregnancies and also express ERα. (Nulliparous, n = 3 mice; third pregnancy, n = 4 mice)

(H) Quantification for *lacZ* labeled epithelium in distal and proximal oviduct across multiple pregnancies (Nulliparous, n = 3 mice; third pregnancy, n = 4 mice; *p = 0.0294; ****p < 0.0001).

(I) Experimental schedule used in (J) to investigate responsiveness of *lacZ*-labeled epithelial cells to tamoxifen administration.

(J) Representative histological images of X-gal-stained mouse oviduct tissue sections showing that *lacZ*-labeled epithelium expands in response to tamoxifen (vehicle, n = 3 mice; tamoxifen, n = 4 mice).

(K) Quantification for *lacZ* labeled epithelium in distal and proximal oviduct after tamoxifen administration (vehicle, n = 3 mice; tamoxifen, n = 4 mice; ***p = 0.0005; ****p < 0.0001).

(L) Representative images showing oviductal organoids derived from *Cspg4^{Cre};R26-lacZ$^{fl/+}$* mice are partially and fully labeled with *lacZ* (n = 4 mice).

(M) Quantification of *lacZ*-labeled organoids from mutant oviduct epithelium (n = 3 mice). Data represent means ± SEM; p values are indicated; two-way ANOVA with Sidak's test. White arrowheads point to $Cspg4^+$ pericytes in (B). In (E), $PAX8^+$, $βgal^+$, $βgal^+AcTub^+$, and $βgal^+$ $AcTub^+$ cells are marked with white, blue, yellow, and pink arrowheads, respectively. Asterisk in (L) denote organoids negative for X-gal staining. Black arrows in (C), (G), and (J) point to *lacZ$^+$* epithelial cells. bv, blood vessel; c, collection; MD, müllerian duct; ut, uterus; od, oviduct; ode, oviductal epithelium; odm, oviductal mesenchyme; o, ovary; preg, pregnancy; PND, postnatal day. Scale bars, 100 μm.

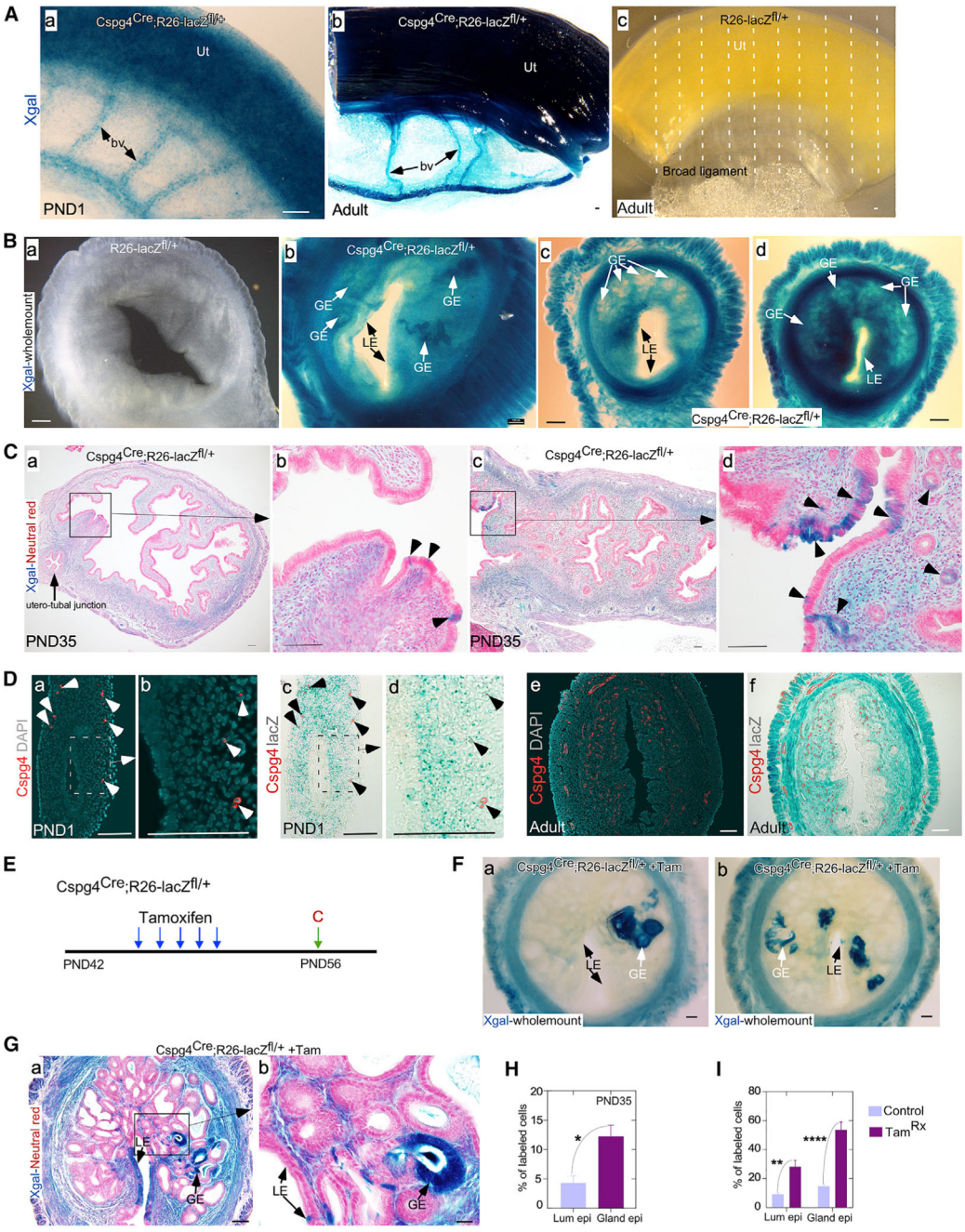

Figure 3. *Cspg4Cre*-Driven, LacZ-Labeled Cells Are Present in the Uterine Epithelium of Nulliparous Mice

(A) X-gal-stained whole-mount images of neonatal (PND1) (a) and adult (b) *Cspg4^{Cre};R26-lacZ$^{fl/+}$* mice uteri. Control uteri depicted no X-gal staining (c). White, dotted lines mark the scheme of serial thick sectioning (125 μm) of the uterus. (PND1, n = 5 mice; adult, n = 5 mutant and 3 control mice).

(B) X-gal staining of 125-μm-thick uterine tissue slices showing that *lacZ^{+}* cells are dispersed in both luminal and glandular epithelium (b–d). No staining in controls (a).

(C) Histological sections showing the distribution of X-gal-positive cells (a–d) (n = 3 mice).

(D) Immunostaining for *Cspg4* in tissue sections of X-gal-stained neonatal (PND1) (a–d) and adult (e and f) *Cspg4*^{Cre};*R26-lacZ*$^{fl/+}$ mice uteri, showing that CSPG4 expression is restricted to stromal perivascular cells (n = 5 mice).

(E) Experimental schedule used in (F) to investigate responsiveness of *lacZ*-labeled epithelial cells to tamoxifen administration.

(F) X-gal staining of 125-μm-thick uterine tissue slices (a and b) showing that *lacZ*-labeled uterine epithelium expands in response to tamoxifen treatment and is more readily visible. (n = 4 mice).

(G) Histology of thick sections presented in (F). (n = 4 mice).

(H) Quantification for *lacZ*-labeled luminal and glandular epithelium at PND35 uterus (n = 3 mice; *p = 0.0235).

(I) Quantification for *lacZ*-labeled luminal and glandular uterine epithelium after tamoxifen administration (vehicle, n = 3 mice; tamoxifen, n = 4 mice; **p = 0.0055; ****p < 0.0001). Data represent means ± SEM; p values are indicated; unpaired t test (H), two-way ANOVA with Sidak's test (I). Black arrowheads in (C) point to *lacZ*$^{+}$ epithelial cells. White and black arrowheads in (D) point to CSPG4^{+} perivascular cells. bv, blood vessel; c, collection; GE, glandular epithelium; LE, luminal epithelium; Tam, tamoxifen; Ut, uterus; PND, postnatal day. Scale bars, 100 μm.

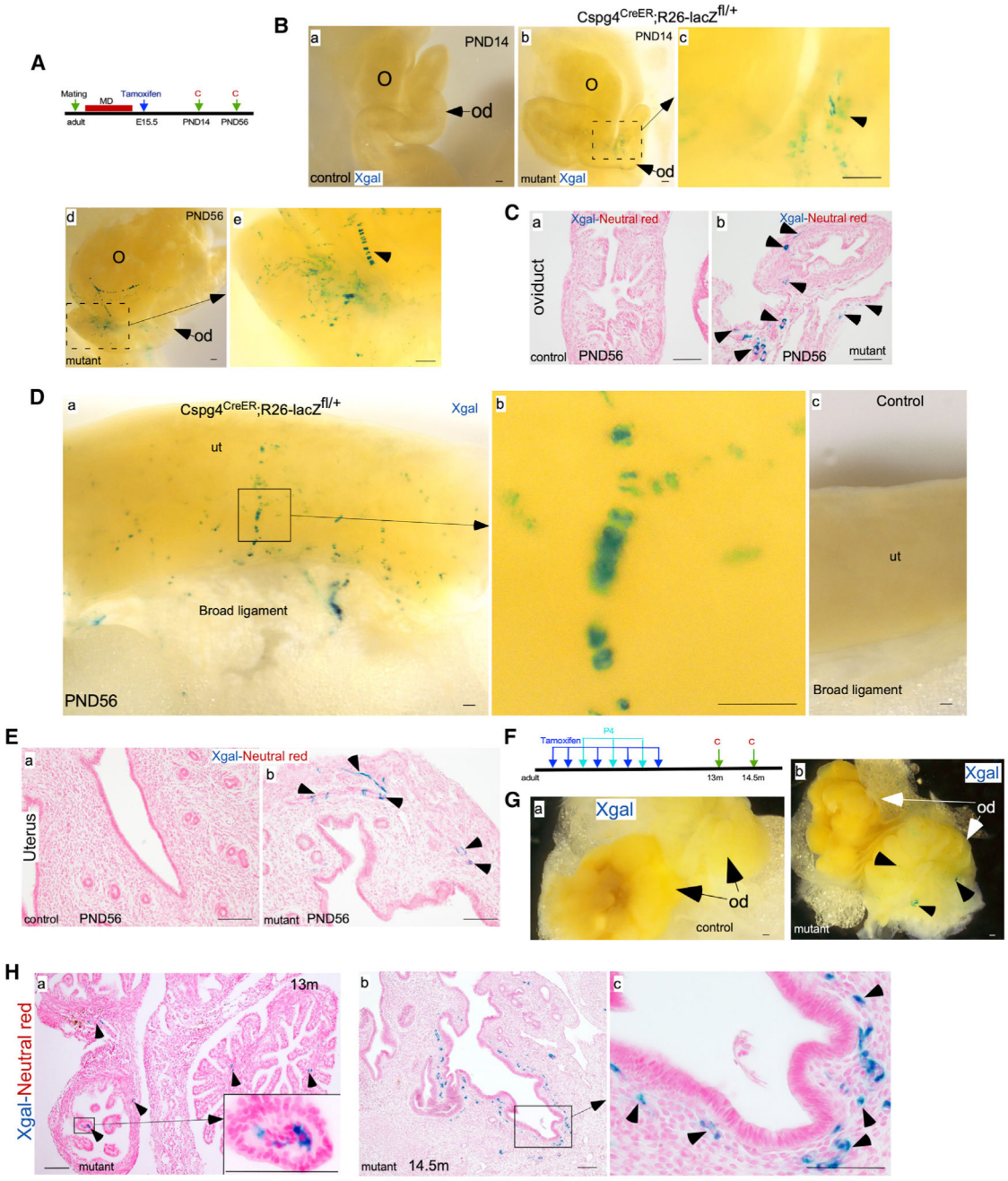

Figure 4. Induction of *Cspg4Cre*-Driven Recombination after Müllerian Duct Development and in Adult FRT Does Not Label Epithelial Cells

(A) Schematic depicting the timeline of tamoxifen administration in *Cspg4*^{CreER}*;R26-lacZ*$^{fl/+}$ mice for labeling CSPG4^{+} cells and subsequent tissue collection (embryonic labeling).

(B) Representative gross images of X-gal-stained oviducts showing *lacZ* expression (black arrowheads in c and e) in perivascular cells in mutants (b–e) but not in controls (a). (PND14, n = 10 mutant and 4 control mice; PND 56, n = 6 mutant and 9 control mice).

(C) Histology images depicting *lacZ* expression in perivascular areas of mutant (black arrowheads in b) but not control (a) oviducts (PND14, n = 10 mutant and 4 control mice; PND 56, n = 6 mutant and 9 control mice).
(D) Gross images of mutant (a and b) and control (c) uteri after X-gal staining (PND14, n = 10 mutant and 4 control mice; PND 56, n = 6 mutant and 9 control mice).
(E) Histological analysis depicting *lacZ* expression in perivascular areas of mutant (black arrowheads in b) but not control (a) (PND14, n = 10 mutant and 4 control mice; PND 56, n = 6 mutant and 9 control mice).
(F) Schematic depicting the time line of tamoxifen administration in $Cspg4^{CreER};R26\text{-}lacZ^{fl/+}$ mice for labeling CSPG4^{+} cells and subsequent tissue collection (adult labeling).
(G) Gross images of oviducts from control (a) and mutant (b) mice after X-gal staining (black arrowheads point to $lacZ^{+}$ cells) (13 m, n = 5 mice; 14.5 m, n = 4 mice)
(H) Histological images of mutant oviducts and uteri post-labeling at 13 m (a) and 14.5 m (b and c) chase points (black arrowheads point to $lacZ^{+}$ cells) (13 m, n = 5 mice; 14.5 m, n = 4 mice).
Black arrowheads point to $lacZ^{+}$ cells. Black box and dashed boxes mark the area for the high-magnification images. c, collection; P4, progesterone; MD, müllerian duct; ut, uterus; od, oviduct; o, ovary; PND, postnatal day. Scale bars, 100 μm.

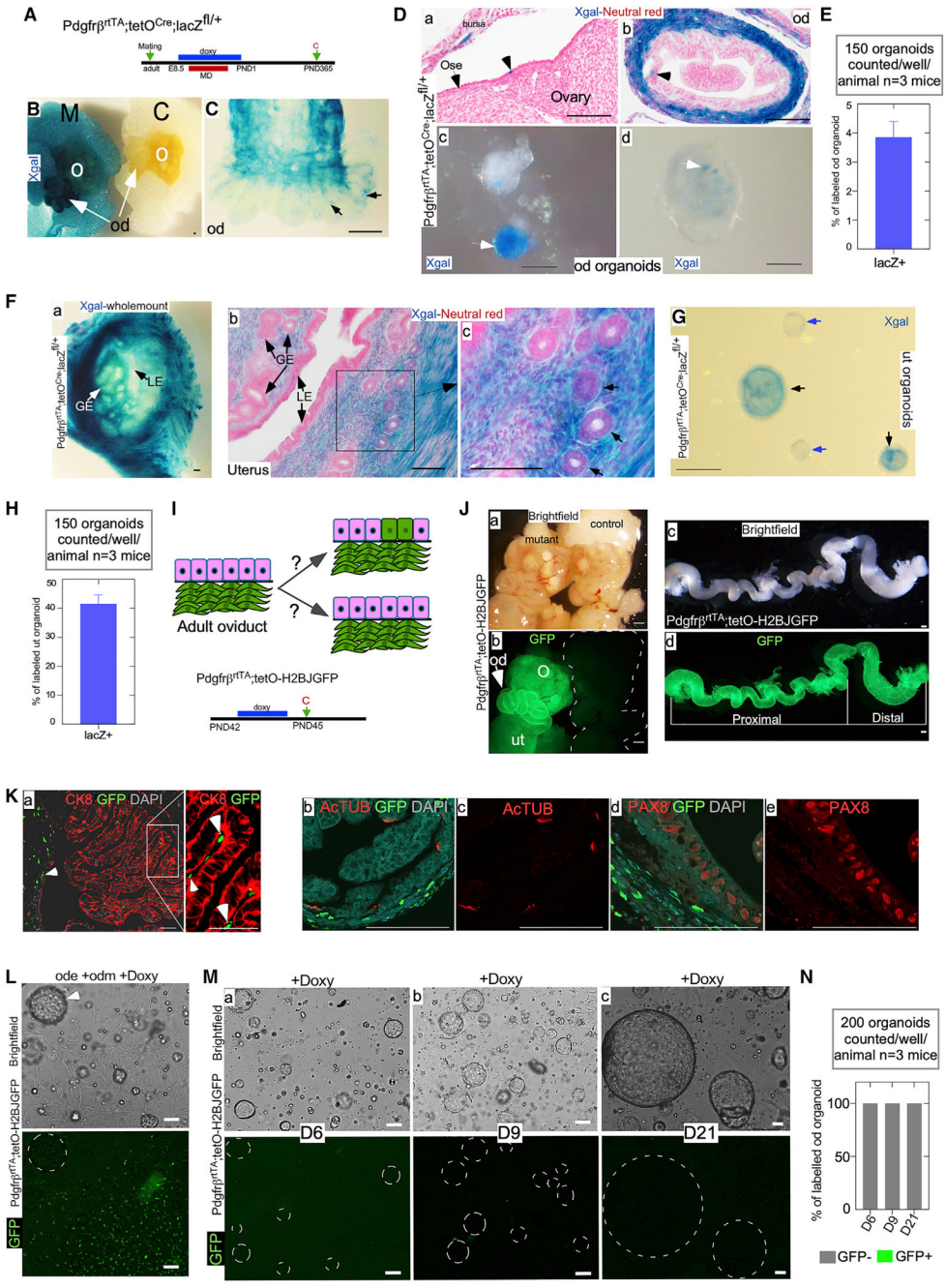

Figure 5. *Pdgfrβ Cre* Is Active in the Müllerian Duct Epithelium but Not in Adult FRT Epithelium

(A) Schematic depicting the time line of doxycycline administration and subsequent tissue collection in *Pdgfrβ*^{rtTA}*;tetO*^{Cre}*;R26-lacZ*$^{fl/+}$ mice for labeling PDGFRβ^{+} cells during Müllerian duct formation (embryonic labeling).

(B) Gross images of X-gal-stained ovaries and oviducts showing the presence of *lacZ*$^{+}$ cells in the mutant (M) ovary, ovarian fat, and oviducts, but not in controls (C) (n = 3 mutant and 3 control mice).

(C) A gross image of X-gal-stained, mutant fimbriae showing the presence of *lacZ*$^{+}$ cells (black arrows) (n = 3 mutant and 3 control mice).
(D) Representative histological images showing *lacZ*$^{+}$ cells (black arrowheads) in ovarian surface epithelium (a) and oviductal epithelium (b). Representative gross images of X-gal-stained organoids derived from mutant oviducts showing the presence of *lacZ*$^{+}$ cells (white arrows) (c and d) (n = 3 mice).
(E) Quantification of *lacZ* -labeled organoids from mutant oviduct epithelium (n = 3 mice).
(F) Representative images of X-gal-stained, 125-μm-thick uterine-tissue slices and tissue sections from the same experiment as depicted in (A). Histological images showing *lacZ*$^{+}$ cells (black arrows) were also present in mutant glandular epithelial cells (b and c) (n = 3 mice).
(G) Representative gross images of X-gal-stained organoids derived from mutant uterine epithelium, showing the presence of both *lacZ*$^{+}$ (black arrows) and *lacZ*$^{-}$ (blue arrows) organoids (n = 3 mice).
(H) Quantification of *lacZ*-labeled organoids from mutant uterine epithelium (n = 3 mice).
(I) Schematic depicting the two possible theoretical outcomes of tracing the fate of adult-labeled PDGFRβ^{+} cells, and experimental time line of doxycycline administration and subsequent tissue collection in adult *Pdgfrβ*^{rtTA}*;tetO-H2BJGFP* mice for labeling and tracing PDGFRβ^{+} cells.
(J) Representative brightfield and fluorescence images of whole-mount oviducts, ovary, and uterus showing high-GFP expression in mutants but not in controls (a–d) (n = 4 mice).
(K) Immunostaining for GFP (a, b, and d), CK8 (a), Ac-TUB (b and c), and PAX8 (d and e) in adult *Pdgfrβ*^{rtTA}*;tetO-H2BJGFP* oviducts showing GFP expression in the stroma but not in the CK8, Ac-TUB or PAX8 expressing epithelial cells (n = 4 mice).
(L) Representative brightfield and fluorescence images of the oviductal epithelial and stromal cell co-cultured *in vitro*, showing that GFP expression is limited to stromal cells(n = 3 mice).
(M) Representative brightfield and fluorescence images of mutant oviductal organoids cultured for 21 days depicting the absence of GFP expression in these organoids (n = 3 mice).
(N) Quantification showing complete absence of GFP^{+}-oviduct epithelial organoids during the whole culture period (n = 3 mice).
Data represent means ± SEM, white arrowheads in (K) point to GFP^{+} cells in stroma and, in (L), point to oviductal organoids. c, collection; C, control; Doxy, doxycycline; GE, glandular epithelium; LE, luminal epithelium; M, mutant; MD, müllerian duct; ut, uterus; od, oviduct; ode, oviductal epithelium; odm, oviductal mesenchyme; Ose, ovarian surface epithelium; o, ovary; PND, postnatal day. Scale bars, 100 μm.

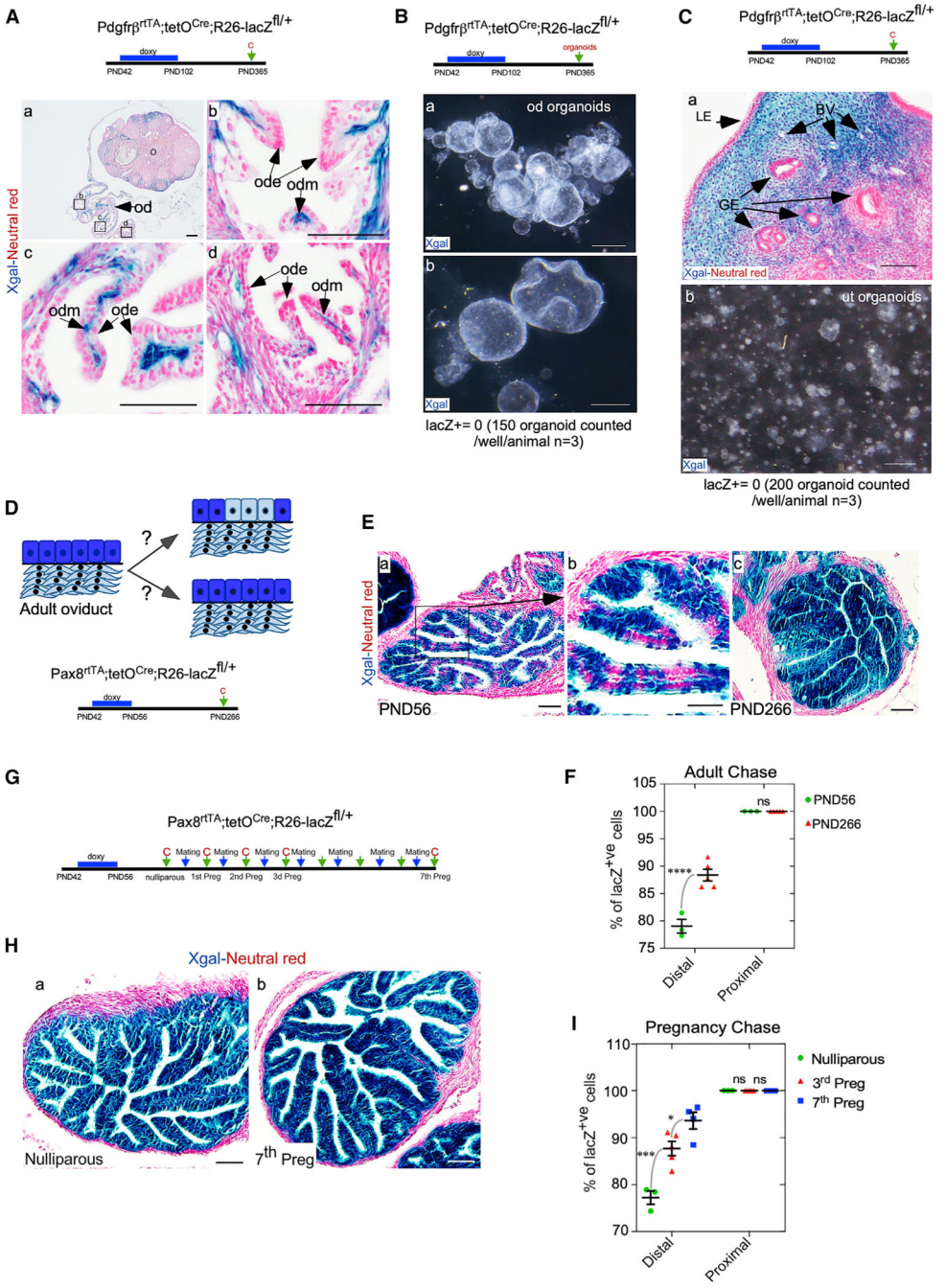

Figure 6. PAX8-Expressing Epithelium-Derived Lineages Rather than PDGFRβ-Derived Mesenchymal Cells Contribute to Oviductal and Uterine Epithelial Lineages

(A) Schematic depicting the timeline of doxycycline administration and subsequent tissue collection in *Pdgfrβ*^{rtTA}*;tetO*^{Cre}*;R26-lacZ*$^{fl/+}$ mice for labeling PDGFRβ^{+} cells during adulthood (adult labeling). Representative histological images of X-gal-stained ovaries and oviducts (low magnification; a) showing *lacZ*$^{+}$ cells in the stroma of mutant oviducts but not in the epithelium (high magnification; b–d). Higher magnifications (b, c, and d) of insets in (a) (PND365, n = 5 mice).

(B) Schematic depicting the timeline of doxycycline administration in *Pdgfrfβ^{rtTA};tetO^{Cre};R26-lacZ$^{fl/+}$* mice and subsequent tissue collection for organoid development. Gross images of X-gal-stained mutant oviductal epithelial organoids revealed absence of any *lacZ^{+}* organoids (a and b) (n = 5 mice).

(C) Experimental plan for *Pdgfrβ^{rtTA};tetO^{Cre};R26-lacZ$^{fl/+}$* mice. Representative histological images of X-gal-stained *Pdgfrβ^{rtTA};tetO^{Cre};R26-lacZ$^{fl/+}$* uteri and gross images of X-gal-stained mutant uterine organoids, showing the complete absence of lacZ^{+} cells in both uterine epithelium and organoids (n = 5 mice).

(D) Schematic depicting the two possible theoretical outcomes of tracing the fate of adult-labeled PAX8^{+} cells, and experimental timeline of doxycycline administration and subsequent tissue collection in adult *Pax8^{rtTA};tetO^{Cre};R26-lacZ$^{fl/+}$* mice for labeling and tracing PAX8^{+} cells.

(E) X-gal staining and quantification of labeling index revealed a stable index of lacZ labeling in the proximal oviductal epithelium with advancing age (PND266), but a progressive increase was seen in the distal oviductal epithelium. (PND56, n = 3 mice; PND266, n = 5 mice).

(F) Quantification of *lacZ^{+}* cells in oviducts at different chase time points (PND56, n = 3 mice; PND266, n = 5 mice; ****$p < 0.0001$; $^{ns}p > 0.9999$).

(G) Schematic depicting the timeline of doxycycline administration and subsequent tissue collection in adult *Pax8^{rtTA};tetO^{Cre};R26-lacZ$^{fl/+}$* mice for labeling and tracing PAX8^{+} cells across multiple pregnancies.

(H) X-gal staining and quantification of labeling index revealed a stable index of *lacZ* labeling in the proximal oviductal epithelium across pregnancies, and an increase in the labeling index of distal oviductal epithelium (a and b); (nulliparous, n = 3 mice; third pregnancy, n = 5 mice; seventh pregnancy, n = 4 mice).

(I) Quantification of *lacZ^{+}* cells in mutant oviducts across pregnancies (nulliparous, n = 3 mice; third pregnancy, n = 5 mice; seventh pregnancy, n = 4 mice; *$p = 0.0132$; ***$p = 0.0001$; $^{ns}p > 0.9999$).

Data represent means ± SEM; p values are indicated; two-way ANOVA with Sidak's test (F) two-way ANOVA with Tukey's test (I). BV, blood vessel; c, collection; doxy, doxycycline; ut, uterus; od, oviduct; ode, oviductal epithelium; odm, oviductal mesenchyme; o, ovary; preg, pregnancy; PND, postnatal day. Scale bars, 100 μm.

KEY RESOURCES TABLE

REAGENT or RESOURCE	SOURCE	IDENTIFIER
Antibodies		
Chicken anti-GFP	Abcam	Cat#ab13970; RRID: AB_300798
Rabbit anti-CSPG4	Millipore	Cat#AB5320; RRID: AB_11213678
Rabbit anti-PAX8	Proteintech Group	Cat#10336-1-AP; RRID: AB_2236705
Rabbit anti-Actub	Abcam	Cat#ab15580; RRID: AB_443209
Rabbit anti-ERα (MC-20)	Santa Cruz Biotechnology	Cat#sc-sc-542; RRID: AB_631064
Rabbit anti-PDGFRβ (28E1)	Cell Signaling Technology	Cat#3169, RRID: AB_2162497
Rat anti-Keratin8	Developmental Studies Hybridoma Bank	Cat#TROMA-I; RRID: AB_531826
Rabbit anti-b-galactosidase	Life Technologies	Cat#A11132; RRID: AB_221539
Mouse anti-Actin, alpha-smooth muscle-Cy3 (Clone 1A4)	Sigma-Aldrich	Cat#C6198; RRID: AB_476856
Rabbit mAb Vimentin (D21H3) XP	Cell Signaling Technology	Cat# 5741, RRID: AB_10695459
Alexa Fluor 488 goat anti-rat IgG ($F(ab')_2$)	Jackson ImmunoResearch Labs	Cat#112-545-072; RRID: AB_2338359
Alexa Fluor 594 goat anti-mouse IgG ($F(ab')_2$) (H + L)	Jackson ImmunoResearch Labs	Cat#115-585-072; RRID: AB_2338879
Alexa Fluor 488 goat anti-chicken IgY (H + L)	Jackson ImmunoResearch Labs	Cat#103-545-155; RRID: AB_2337390
Peroxidase goat anti-rabbit IgG ($F(ab')_2$)	Jackson ImmunoResearch Labs	Cat#111-036-047; RRID: AB_2337945
Peroxidase goat anti-mouse IgG ($F(ab')_2$)	Jackson ImmunoResearch Labs	Cat#115-065-072; RRID: AB_2338565
Chemicals, Peptides, and Recombinant Proteins		
Pronase	Sigma-Aldrich	Cat#10165921001
DNase I	Sigma-Aldrich	Cat#10104159001
Fetal Bovine Serum	Bovogen	Cat#SFBS-F
L-glutamine	HyClone	Cat#SH30034.01
Penicillin-streptomycin	Thermo Fisher Scientific	Cat#15070-063
Matrigel: Cultrex® Reduced Growth Factor Basement Membrane Matrix	Trevigen	Cat#3433-010-01
ITS liquid media supplement	Sigma-Aldrich	Cat#I3146
SB431542 TGF beta inhibitor	Selleckchem	Cat#S1067
GlutaMAX (100X)	Thermo Fisher Scientific (GIBCO)	Cat#35050-061
Ultra serum-G	PALL	Cat#15950-017
B27 supplement	Thermo Fisher Scientific (GIBCO)	Cat#12587-010
N-2 supplement	Thermo Fisher Scientific (GIBCO)	Cat#17502-048
Nicotinamide	Sigma-Aldrich	Cat#N0636
Mouse EGF recombinant	Sigma-Aldrich	Cat#SRP3196
Human FGF-10	Peprotech	Cat#100-26
A83-01	Tocris	Cat#2939
TrypLE express	Thermo Fisher Scientific (GIBCO)	Cat#12604-021
Protein Block Serum Free (Lot#10096977)	DAKO	Cat#X0909
Ab Diluent with Background Reducing Compoents (Lot#10090973)	DAKO	Cat#S3022
Doxycycline hyclate (lot#086M4035V)	Sigma-Aldrich	Cat#D9891

REAGENT or RESOURCE	SOURCE	IDENTIFIER
Neutral Red	Sigma-Aldrich	Cat#72210
Y-27632 dihydrochloride	Tocris	Cat#1254
DMEM/F12 HAM	Sigma-Aldrich	Cat#D8437
HBSS/Modified	HyClone	Cat#SH30031.02
Tamoxifen (Lot#SLBF8049V)	Sigma-Aldrich	Cat#T5648; CAS#10540-29-1
Progesterone (Lot#SLBG1644V)	Sigma-Aldrich	Cat#P 0130; CAS#57-83-0
DAPI dilactate	Sigma-Aldrich	Cat#D9564
Paraformaldehyde 16% solution EM Grade	Electron Microscopy Sciences	Cat#15710
Xgal (Lot#ES531-B061890)	Bioline	Cat#BIO-37035
Critical Commercial Assays		
EnVision™+ Dual Link System-HRP (DAB^+) (Lot#10095442)	DAKO	Cat#K4065
RNAscope 2.5 HD Assay-RED kit	Advanced Cell Diagnostics	Cat#322350
RNAscope 2.5 HD Detection Reagents-RED	Advanced Cell Diagnostics	Cat#322360
RNAscope H202 & Protease Plus Reagents	Advanced Cell Diagnostics	Cat#322330
Experimental Models: Cell Lines		
L-WRN cells	ATCC	Cat#CRL-3276; RRID: CVCL_DA06
Experimental Models: Organisms/Strains		
Mouse: *Pax8*^{rtTA}: B6.Cg-Tg(Pax8-rtTA2S*M2)1Koes/J	The Jackson Laboratory	JAX:007176; RRID:IMSR_JAX:007176
Mouse: *tetO*^{Cre}: STOCK Tg(tetO-cre)1Jaw/J	The Jackson Laboratory	JAX:006224; RRID:IMSR_JAX:006224
Mouse: *tetO*^{H2BJGFP}: STOCK Tg(tetO-HIST1H2BJ/GFP) 47Efu/J	The Jackson Laboratory	JAX:005104; RRID:IMSR_JAX:005104
Mouse: *R26-lacZ*$^{fl/fl}$: B6.129S4-Gt(ROSA)26Sor^{tm1Sor}/J	The Jackson Laboratory	JAX:003474; RRID:IMSR_JAX:003474
Mouse: *B6;129S7-Amhr2tm3(cre)Bhr/Mmnc*	Mutant mouse resource and research centers supported by NIH (MMRRC)	014245-UNC; RRID:MMRRC_014245-UNC
Mouse: *Amhr2tm2(lacZ)Bhr*	Arango et al., 2008	MGI:5515927
Mouse: B6;FVB-Ifi208Tg(Cspg4-cre)1Akik/J	The Jackson Laboratory	JAX:008533; RRID:IMSR_JAX:008533
Mouse: B6.Cg-Tg(Cspg4-cre/Esr1*)BAkik/J	The Jackson Laboratory	JAX:008538; RRID:IMSR_JAX:008538
Mouse: C57BL/6-Tg(Pdgfrb-rtTA)58Gpta/J	The Jackson Laboratory	JAX:028570; RRID:IMSR_JAX:028570
Oligonucleotides		
RNAscope Negative Control Probe - DapB	Advanced Cell Diagnostics	Cat#310043
RNAscope Positive Control Probe - Mm-Ppib	Advanced Cell Diagnostics	Cat#313911
RNAscope Probe-Mm-Amhr2	Advanced Cell Diagnostics	Cat#489821
Software and Algorithms		
ImageJ	Schneider et al., 2012	https://imagej.nih.gov/ij/
Zen Black 2014 SP1 64-bit (version 9.2.6.54)	Zeiss (Jena, Germany)	https://www.zeiss.com/microscopy/int/products/microscope-software/zen-lite.html
GraphPad Prism version 7.02	GraphPad Software, La Jolla California USA	https://www.graphpad.com